

AD-A163 708 ON THE TWO-DIMENSIONAL PERIODIC SURFACE WAVES OCCURRING 1/1

141

IN RECTANGULAR VE. (U) WISCONSIN UNIV-MADISON

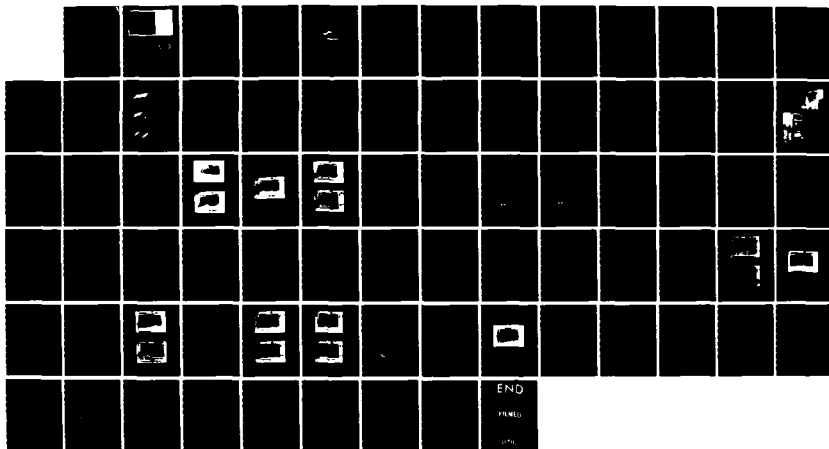
MATHEMATICS RESEARCH CENTER T J BRIDGES OCT 85

UNCLASSIFIED MRC-TSR-2878 DAAG29-80-C-0041

MRC-TSR-2878 DAAG29-80-C-0041

F/G 20/4

NL





MICROCOPY RESOLUTION TEST CHART
NATIONAL BUREAU OF STANDARDS-1963-A

2

AD-A163 708

MRC Technical Summary Report #2878

ON THE TWO-DIMENSIONAL PERIODIC SURFACE
WAVES OCCURRING IN RECTANGULAR VESSELS:
THEORY VERSUS EXPERIMENT

Thomas J. Bridges

MIPAC Facility Document No. 4

Mathematics Research Center
University of Wisconsin—Madison
610 Walnut Street
Madison, Wisconsin 53705

October 1985

(Received October 4, 1985)

DTIC
ELECTE
FEB 5 1986
S B D

DTIC FILE COPY

Approved for public release
Distribution unlimited

Sponsored by

U. S. Army Research Office
P. O. Box 12211
Research Triangle Park
North Carolina 27709

National Science Foundation
Washington, DC 20550

86 2 5

037

UNIVERSITY OF WISCONSIN-MADISON
MATHEMATICS RESEARCH CENTER

**ON THE TWO-DIMENSIONAL PERIODIC SURFACE WAVES
OCCURRING IN RECTANGULAR VESSELS:
THEORY VERSUS EXPERIMENT**

Thomas J. Bridges

Technical Summary Report #2878
October 1985

ABSTRACT

This paper is a four part dialectic between theory and experimental observations and measurements of two dimensional periodic surface waves in a vessel of rectangular cross section. The first two parts consist of minor contributions to the existing theory and experimental measurements of elliptic (deep water) standing waves and the (shallow water) travelling hydraulic jump. A new theory is proposed in the third part which explains the transition from the elliptic standing wave to the hyperbolic travelling hydraulic jump. The result is a family of standing cnoidal waves. To lowest order the solution is composed of two non-interacting periodic progressive cnoidal waves travelling in opposite directions. At higher order the two wave trains interact but the interaction produces nothing of qualitative significance except when the cnoidal standing wave of highest amplitude is considered. This family of waves is validated by experimental observation in part four. In addition in part four observation of compound cnoidal standing waves leads to a conjecture about a sequence of continuous wave forms in parameter space leading from the linear sinusoidal wave to the travelling hydraulic jump. /

AMS (MOS) Subject Classifications: 76B15, 35B10, 35B32, 35R35

Key Words: standing waves, cnoidal waves, bifurcation, experimental observations

Work Unit Number 2 (Physical Mathematics)

Sponsored by the United States Army under Contract No. DAAG29-80-C-0041. This material is based upon work supported by the National Science Foundation under Grant No. DMS-8210950, Mod. 1.

Thomas J. Bridges

The theory will be concerned with an idealized fluid: i.e. inviscid and irrotational and without surface tension at the surface. The rectangular vessel of length $2a$ containing fluid of still water level h , when a forcing function is present, rotates harmonically about a fixed point. Such a configuration is depicted in Figure 1.1. The parameters d and γ fix the point of rotation, θ is the rotary displacement at frequency ω of the vessel. Under the conditions specified the governing equations are,

$$\frac{\partial \phi}{\partial y} = \Omega x \quad \text{on } y = -h \quad (1.2b)$$

Sponsored by the United States Army under Contract No. DAAG29-80-C-0041. This material is based upon work supported by the National Science Foundation under Grant No. DMS-8210950, Mod 1.



Dist	Special
A-1	

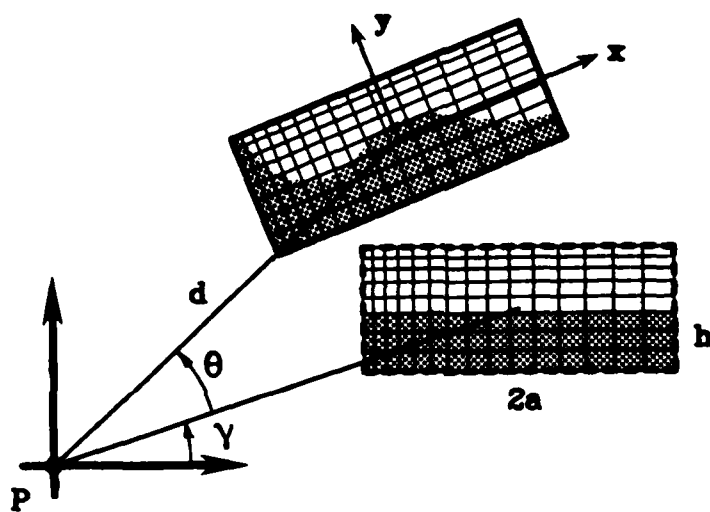


Figure 1.1 A schematic of the two-dimensional wave field in a rotating vessel with rectangular cross-section.

and on $y = \eta(x, t)$

$$\frac{\partial \eta}{\partial t} + \frac{\partial \phi}{\partial x} \frac{\partial \eta}{\partial x} + \Omega \eta \frac{\partial \eta}{\partial x} - \frac{\partial \phi}{\partial y} + \Omega x = 0 \quad (1.3)$$

$$\begin{aligned} \frac{\partial \phi}{\partial t} + \frac{1}{2} \left[\left(\frac{\partial \phi}{\partial x} \right)^2 + \left(\frac{\partial \phi}{\partial y} \right)^2 \right] + \Omega \left(\eta \frac{\partial \phi}{\partial x} - x \frac{\partial \phi}{\partial y} \right) + \frac{1}{2} \Omega^2 (\eta^2 + x^2) \\ + \eta \left[g \cos \theta + \dot{\Omega} d \cos \gamma - \Omega^2 d \sin \gamma \right] + x \left[g \sin \theta - \dot{\Omega} d \sin \gamma - \Omega^2 d \cos \gamma \right] = 0 \end{aligned} \quad (1.4)$$

where ϕ is the velocity potential and η is the surface displacement, and $\Omega = \dot{\theta}$, the angular velocity of the vessel. The derivation of these equations, under the assumption of a uniform vorticity field, is given in Appendix I.

In the absence of the forcing function the two relevant dimensionless parameters are $\delta = h/2a$ and $\epsilon = H/h$ where H is a measure of the wave amplitude above the still water level. The introduction of the forcing function brings in the parameters d , γ , ω , and ϑ where ϑ is the amplitude of the harmonic forcing function θ .

The surface waves may be classified with the parameters ϵ and δ . When $\epsilon \ll \delta^2$ (which includes the case $\epsilon \rightarrow 0$, i.e. linear waves) the surface waves occurring are elliptic standing waves. When $\epsilon \gg \delta^2$ the travelling hydraulic jump occurs. A theory for both these regions has previously been established. A theory for $\epsilon \ll \delta^2$ was established by Tajdbakhsh and Keller[15] and a theory for the region $\epsilon \gg \delta^2$ has been established by Chester[2,3] and Verhagen and Van Wijngaarden[19]. These two theories with improvements are given in Section 2. In Section 3 experimental observations corresponding to the theory in Section 2 are contained. This includes photos and time series for elliptic standing waves and the travelling hydraulic jump. Both of these wave types have been studied and observed in the past. However the region in between has recieved almost no attention.

In Section 4 a theory is proposed for surface waves in the intermediate region when $\epsilon = O(\delta^2)$. The result is that a family of *cnoidal standing waves* exists in this region. Then in Section 5 experimental verification of these waves is discussed along with another class of compound standing waves. It is conjectured that these compound standing waves are combinations of various mode cnoidal standing waves, and as the amplitude is increased higher mode cnoidal standing waves are excited and eventually there is enough harmonics to produce a travelling hydraulic jump. If, in fact, the family of cnoidal standing waves are the only eigenfunctions existing in the intermediate range between the elliptic standing wave and the hydraulic jump the the following scenario can be constructed for the complete range of ϵ, δ when δ is sufficiently small.

When $\epsilon \ll \delta^2$ (and δ small, including the limit as the amplitude goes to zero, i.e. linear waves) an elliptic standing wave forms which bifurcates from the state of rest. This wave is well described by the theory of Tajdbakhsh and Keller. It is a weakly nonlinear wave containing only a few significant harmonics. However this wave breaks down as ϵ approaches δ^2 in magnitude. This may be shown with the solution of Tajdbakhsh and Keller itself but in an interesting piece of work Vanden-Broeck and Schwartz [18] using a numerical scheme have shown that the bifurcation of the natural frequency has a turning point when $\epsilon = O(\delta^2)$ and the theory of Tajdbakhsh and Keller can not get around the turning point. Vanden-Broeck and Schwartz computed numerical solutions for the region outside the turning point and conjectured that there might be a new class of standing waves in this region. By devising a perturbation scheme for small ϵ and δ such that the ratio ϵ to δ^2 is constant, it is found in Section 4 that this, in fact, is where the family of cnoidal standing waves lives. These waves are much richer harmonically as they have a complete Fourier series.

As the amplitude is increased further the class of solutions observed are combinations of the set of cnoidal standing waves selected by the forcing function. Observance of this phenomena in the experiment suggests that as ϵ is increased beyond δ^2 the natural frequencies of the higher mode cnoidal standing waves become integral multiples of the fundamental in sequence. First the 3-mode is excited and a compound 1-3 mode cnoidal standing wave is observed. As the amplitude is increased further relative to δ^2 a 5-mode is added to the wave form and this forms the compound wiggle wave discussed in Section 5. Further increase of the amplitude introduces higher and higher harmonics until eventually the wave field jumps to the travelling hydraulic jump. Interestingly, this cascading process, unlike turbulence for example, is not dynamic. At a fixed amplitude each compound wave in the sequence is (apparently) stable as evidenced by the results in Section 5. Therefore this sequence of compound standing waves is a sequence of equilibrium states in parameter space which eventually leads to that flood of harmonics; the travelling hydraulic jump.

Obviously much work remains to substantiate these claims but it does suggest a continuity in parameter space between sinusoidal waves and the hydraulic jump. However as evidence of the lack of concrete and rigorous theory in this area there has not even been an existence proof for elliptic standing waves when $\epsilon \ll \delta^2$ but ϵ still finite. So much work remains to be done on this problem.

2. Theory - I: Elliptic Standing Waves and Hydraulic Jumps

2.1 Introduction

There are essentially two existing theories describing the nonlinear waves in a rectangular basin. The first is the theory of Tadjbakhsh and Keller [15] which finds the linear eigenvalues and the standing wave solutions emitted by them. These waves will be referred to as *elliptic standing waves* since they are governed by an elliptic partial differential equation. It will be shown however that these waves are valid for only a small range of amplitude, breaking down when $\epsilon = O(\delta^2)$.

The other theory is that proposed by Chester [2,3] and Verhagen and Van Wijngaarden [19]. They consider the region where $\epsilon \gg \delta^2$ (shallow water, finite amplitude) and find that there are no periodic solutions in this region because dispersion is negligible here. But the introduction of a forcing function renders the problem solvable. Periodic solutions which are discontinuous may be found in this case. The discontinuous solutions represent a family of travelling hydraulic jumps. It is interesting to note that the hydraulic jump is not an eigenfunction. It is, sort of, a state of degeneracy, where all the standing wave modes coalesce to form this odd wave.

These two theories, however, leave a void in the region $\epsilon = O(\delta^2)$. A theory is proposed in Section 4 for this region. It is found that a family of *cnoidal standing waves* exists in this region.

First, the theory of Tadjbakhsh and Keller will be given with some embellishment. Their analysis was for the fundamental mode only. Here it is extended to arbitrary mode number. The main results only will be given, the details of the procedure can be found in their paper.

2.2 Elliptic Standing Waves

The independent and dependent variables are scaled in the following way: $x \rightarrow 2a$, $y \rightarrow h$, $t \rightarrow 1/\omega$, $\omega \rightarrow \sqrt{gh}/2a$, $\eta \rightarrow \epsilon h$, and $\phi \rightarrow \epsilon 2a\sqrt{gh}$, where $2a$ is the tank length, h the still water depth, and the dimensionless parameters are $\epsilon = H/h$ and $\delta = h/2a$, where H is a measure of the maximum height of a wave above the still water level. This scaling is appropriate for fluid of finite depth only and must be recast for the case of infinite depth. The governing set of equations and boundary conditions, when the forcing function is absent, are,

$$\delta^2 \frac{\partial^2 \phi}{\partial x^2} + \frac{\partial^2 \phi}{\partial y^2} = 0 \quad \text{for } -\frac{1}{2} \leq x \leq \frac{1}{2}, -1 \leq y \leq \epsilon \eta(x, t) \quad (2.1)$$

$$\frac{\partial \phi}{\partial x} = 0 \quad \text{at } x = \pm \frac{1}{2} \quad (2.2a)$$

$$\frac{\partial \phi}{\partial y} = 0 \quad \text{at } y = -1 \quad (2.2b)$$

$$\omega \frac{\partial \eta}{\partial t} + \epsilon \frac{\partial \eta}{\partial x} \frac{\partial \phi}{\partial x} - \frac{1}{\delta^2} \frac{\partial \phi}{\partial y} = 0 \quad \text{on } y = \epsilon \eta(x, t) \quad (2.3a)$$

$$\omega \frac{\partial \phi}{\partial t} + \frac{\epsilon}{2} \left[\left(\frac{\partial \phi}{\partial x} \right)^2 + \frac{1}{\delta^2} \left(\frac{\partial \phi}{\partial y} \right)^2 \right] + \eta = 0 \quad \text{on } y = \epsilon \eta(x, t) \quad (2.3b)$$

To obtain a formal solution to this problem in the limit as ϵ tends to zero, a power series solution in ϵ is sought,

$$\phi = \phi_0 + \epsilon \phi_1 + \epsilon^2 \phi_2 + \dots \quad (2.4a)$$

$$\eta = \eta_0 + \epsilon \eta_1 + \epsilon^2 \eta_2 + \dots \quad (2.4b)$$

$$\omega = \omega_0 + \epsilon \omega_1 + \epsilon^2 \omega_2 + \dots \quad (2.4c)$$

The free surface boundary conditions are expanded in a Taylor series about $y = 0$, the expressions (2.4) are then substituted into the set (2.1)-(2.3). Equating terms proportional to like powers of ϵ to zero results in the sequence of *elliptic* boundary value problems,

$$\delta^2 \frac{\partial^2 \phi_j}{\partial x^2} + \frac{\partial^2 \phi_j}{\partial y^2} = 0 \quad \text{for } -\frac{1}{2} \leq x \leq \frac{1}{2}, -1 \leq y \leq 0 \quad (2.5)$$

$$\frac{\partial \phi_j}{\partial x} = 0 \quad \text{at } x = \pm \frac{1}{2} \quad (2.6a)$$

$$\frac{\partial \phi_j}{\partial y} = 0 \quad \text{at } y = -1 \quad (2.6b)$$

$$\omega_0 \frac{\partial \eta_j}{\partial t} - \frac{1}{\delta^2} \frac{\partial \phi_j}{\partial y} = R_j \quad \text{at } y = 0 \quad (2.7a)$$

$$\omega_0 \frac{\partial \phi_j}{\partial t} + \eta_j = S_j \quad \text{at } y = 0 \quad (2.7b)$$

for $j = 0, 1, \dots$. The R_j and S_j , which are essentially the same as those found in the paper of Tajdbakhsh and Keller, are dependent on terms of previous order only. For the linear problem $R_0 = S_0 = 0$ and it is straightforward to show that the zeroth order solution is

$$\omega_0 = \sqrt{\frac{\alpha_m}{\delta} \tanh \alpha_m \delta} \quad (2.8)$$

$$\eta_0 = \cos \alpha_m \bar{x} \sin t \quad (2.9)$$

$$\phi_0 = \omega_0^{-1} \frac{\cosh \alpha_m \delta (1 + y)}{\cosh \alpha_m \delta} \cos \alpha_m \bar{x} \cos t \quad (2.10)$$

where $\alpha_m = m\pi$, $m = 1, 2, \dots$, and $\bar{x} = x + \frac{1}{2}$. The points ω_0 for each m are the bifurcation points. The higher order terms will then give the solutions along the branches emitted by these points. The approach is straightforward and the details will be omitted.

The first order solution is,

$$\omega_1 = 0 \quad (2.11)$$

$$\eta_1 = [B_{11} + B_{12} \cos 2t] \cos 2\alpha_m \bar{x} \quad (2.12)$$

$$\phi_1 = A_{11} t + A_{12} \sin 2t + A_{13} \frac{\cosh 2\alpha_m \delta (1 + y)}{\cosh 2\alpha_m \delta} \cos 2\alpha_m \bar{x} \sin 2t \quad (2.13)$$

where

$$A_{11} = \frac{1}{\omega_0} (\omega_0^2 \delta^2 - \frac{\alpha_m^2}{\omega_0^2}) \quad (2.14a)$$

$$A_{12} = \frac{1}{16\omega_0} (\frac{\alpha_m^2}{\omega_0^2} + 3\omega_0^2 \delta^2) \quad (2.14b)$$

$$A_{13} = \frac{-3}{16\omega_0} (\omega_0^2 \delta^2 - \frac{\alpha_m^4}{\omega_0^6 \delta^2}) \quad (2.14c)$$

$$B_{11} = \frac{1}{8} (\frac{\alpha_m^2}{\omega_0^2} + \omega_0^2 \delta^2) \quad (2.15a)$$

$$B_{12} = \frac{\alpha_m^2}{8\omega_0^2} (1 - \frac{3\alpha_m^2}{\omega_0^4 \delta^2}) \quad (2.15b)$$

Proceeding to the second order problem, the result is

$$\omega_2 = \frac{\omega_0}{64} \left[\frac{9\alpha_m^6}{\omega_0^8 \delta^2} - \frac{12\alpha_m^4}{\omega_0^4} - 2\omega_0^4 \delta^4 - 3\alpha_m^2 \delta^2 \right] \quad (2.16)$$

$$\begin{aligned} \eta_2 = & \left[B_{21} \cos \alpha_m \bar{x} + B_{22} \cos 3\alpha_m \bar{x} \right] \sin t \\ & + \left[B_{23} \cos \alpha_m \bar{x} + B_{24} \cos 3\alpha_m \bar{x} \right] \sin 3t \end{aligned} \quad (2.17)$$

$$\begin{aligned} \phi_2 = & A_{21} \frac{\cosh 3\alpha_m \delta (1+y)}{\cosh 3\alpha_m \delta} \cos 3\alpha_m \bar{x} \cos t \\ & + A_{22} \frac{\cosh \alpha_m \delta (1+y)}{\cosh \alpha_m \delta} \cos \alpha_m \bar{x} \cos 3t \\ & + A_{23} \frac{\cosh 3\alpha_m \delta (1+y)}{\cosh 3\alpha_m \delta} \cos 3\alpha_m \bar{x} \cos 3t \end{aligned} \quad (2.18)$$

where the coefficients A_{2j} and B_{2j} are given in Appendix II.

Before proceeding to evaluate these solutions some estimate of the range of validity of the solutions is helpful. The appearance of δ^{-2} in the coefficients A_{13} and B_{12} , as well as the frequency correction ω_2 , is ominous as $\delta \rightarrow 0$. Therefore it is apparent the results will be valid for only a finite range of amplitude; $0 \leq \epsilon \leq \epsilon_m(\delta)$. A clue as to the value of $\epsilon_m(\delta)$ can be found by taking the limit of ω as $\delta \rightarrow 0$ with ϵ fixed,

$$\lim_{\substack{\delta \rightarrow 0 \\ \epsilon \text{ fixed}}} \omega = \alpha_m + \frac{9\alpha_m}{64\alpha_m^2} \frac{\epsilon^2}{\delta^2} + \dots \quad (2.19)$$

Obviously, when $\epsilon \sim \alpha_m \delta$ the tenet of the expansion is violated. Namely, higher order terms should be of higher order. This suggests that $\epsilon_m(\delta) = 0(\delta)$. However, applying the same argument to η results in

$$\lim_{\substack{\delta \rightarrow 0 \\ \epsilon \text{ fixed}}} \eta(x, t) = \cos \alpha_m \bar{x} \cos t - \frac{3\epsilon}{8\alpha_m^2 \delta^2} \cos 2\alpha_m \bar{x} \cos 2t \\ - \frac{27\epsilon^2}{256\alpha_m^4 \delta^4} \cos 3\alpha_m \bar{x} \sin 3t + \dots \quad (2.20)$$

Contrary to the frequency, the wave height expansion breaks down when $\epsilon \sim (\alpha_m \delta)^2$. At this point there is a spillover of the higher harmonics onto the zeroth order term, again violating the tenet of the expansion. This results in a lower estimate for the domain of validity in the amplitude of $\epsilon_m(\delta) = 0(\delta^2)$. It can therefore be concluded that the classical standing wave solution is valid for any depth such that $0 \leq \epsilon \leq \epsilon_m(\delta)$ with $\epsilon_m(\delta) = 0(\delta^2)$. In this range the solutions are for *elliptic waves*. The boundary value problem is essentially elliptic with merely a time dependent domain.

The effect of amplitude on the frequency for waves of this type can be seen in the following bifurcation diagrams. Figures 2.1, 2.2, and 2.3 are bifurcation diagrams, for the frequency, at $\delta = .4$, $\delta = .2$, and $\delta = .1$ respectively. The bifurcation is subcritical or supercritical depending on the value of δ . The switch occurs when $\omega_2 = 0$. Setting $\omega_2 = 0$ results in the equation,

$$\tanh^2 \alpha_m \delta = \frac{1}{2} \left[(29 + 4\sqrt{74})^{\frac{1}{5}} + (29 - 4\sqrt{74})^{\frac{1}{5}} - 1 \right] \quad (2.21)$$

Solving this shows that $\omega_2 = 0$ when $\alpha_m \delta \sim 1.0581$. Therefore the first mode switches direction when $\delta \sim .34$, the second when $\delta \sim .17$, and the third when $\delta \sim .11$.

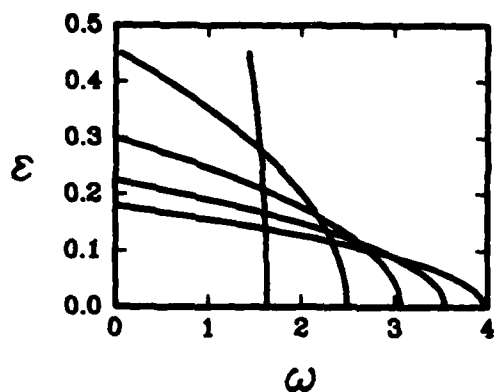


Figure 2.1 Bifurcation diagram for the first five two dimensional elliptic standing wave modes with $\delta = \frac{4}{10}$.

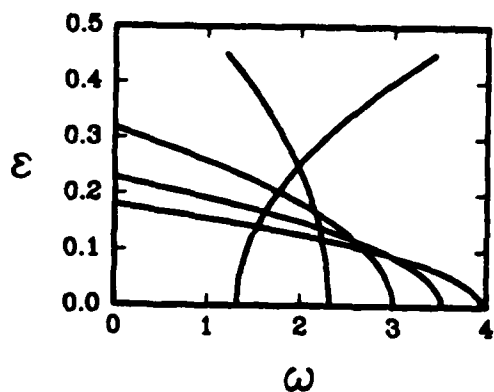


Figure 2.2 Bifurcation diagram for the first five two dimensional elliptic standing wave modes with $\delta = \frac{2}{10}$.

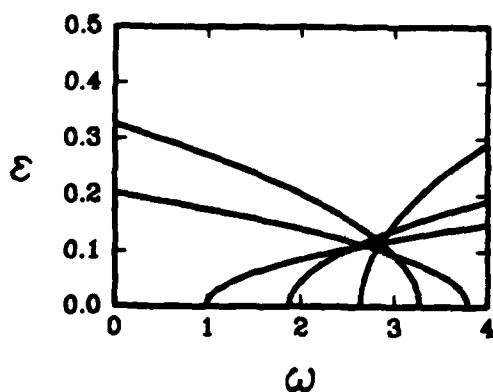


Figure 2.3 Bifurcation diagram for the first five two dimensional elliptic standing wave modes with $\delta = \frac{1}{10}$.

Figures 2.4, 2.5, and 2.6 give examples of the wave height for modes 1, 2, and 3 respectively. They are for $\delta = 0.4$. The solutions are similar at other values of δ and ϵ when $\epsilon < \epsilon_m$. The first mode is the classical standing wave often referred to as the slosh mode, and the second mode is the mode studied by Taylor[16] in his study of the highest standing wave. In Figure 2.7 the wave height at the left tank wall is plotted as a function of time. This time series is typical for the elliptic standing wave when $\epsilon \ll \delta^2$.

As pointed out by Tadjbakhsh and Keller and Concus [6], the above expansion breaks down, even when $\epsilon < \epsilon_m$, if a higher mode becomes an integral multiple of the fundamental. This happens when

$$m \tanh m\pi\delta = p^2 \tanh \pi\delta \quad (2.22)$$

for any positive integer p and $m = 2, 3, \dots$. When the condition (2.22) is met, an internal resonance occurs. In other words higher harmonics of the fundamental generated by the nonlinearity excite other linear modes. When this occurs a separate expansion is necessary.

The condition (2.22) is realized for particular values of δ . There are an infinity of these singularities (this has been shown by Concus [1]), but only the lowest order interactions will be important. However it will be shown that even these are negligible. The first three critical points, where $\sigma_j = \sqrt{j\pi\delta^{-1} \tanh j\pi\delta}$, are

$$\begin{aligned} \sigma_3 = 2\sigma_1 \quad \text{when} \quad \tanh \pi\delta &= \sqrt{\frac{5}{9}}, \text{ i.e., } \delta \sim .306 \\ \sigma_4 = 3\sigma_1 \quad \text{when} \quad \tanh \pi\delta &= \frac{1}{3} \sqrt{2\sqrt{106} - 19}, \text{ i.e., } \delta \sim .143 \\ \sigma_5 = 3\sigma_1 \quad \text{when} \quad \tanh \pi\delta &= \frac{1}{4} \sqrt{\sqrt{832/5} - 8}, \text{ i.e., } \delta \sim .198 \end{aligned}$$

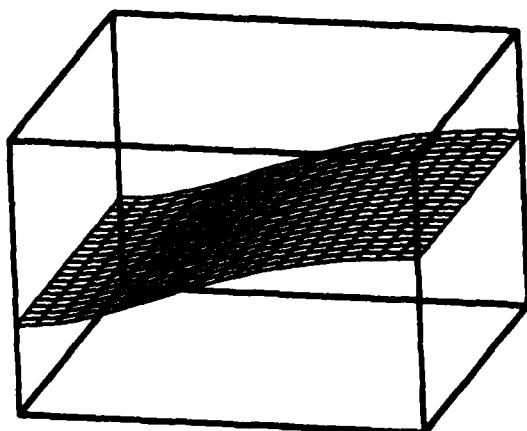


Figure 2.4 Spatial distribution of the wave height, for the first mode, at fixed time with $\delta = \frac{4}{10}$, and $\epsilon = .15$.

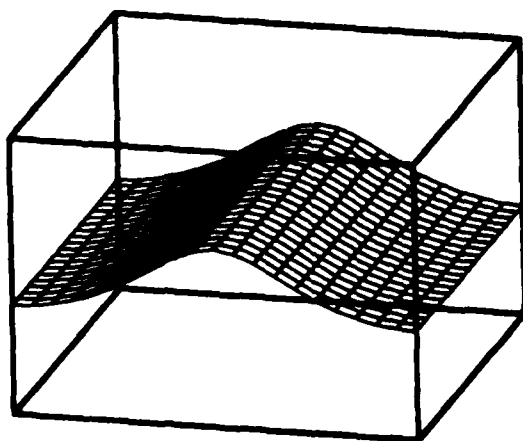


Figure 2.5 Spatial distribution of the wave height, for the second mode, at fixed time with $\delta = \frac{4}{10}$, and $\epsilon = .12$.

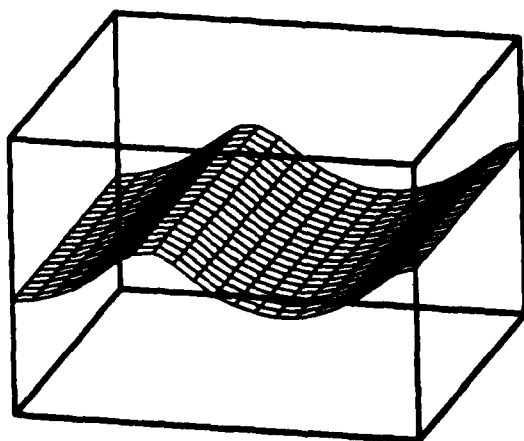


Figure 2.6 Spatial distribution of the wave height, for the third mode, at fixed time with $\delta = \frac{4}{10}$, and $\epsilon = .10$.

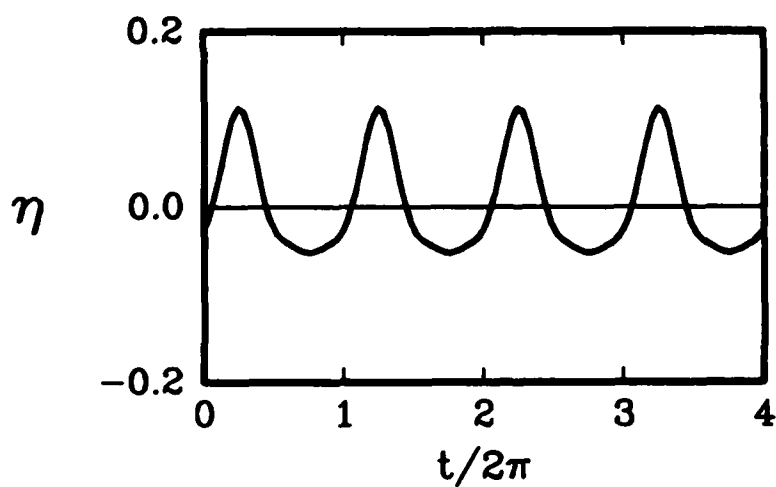


Figure 2.7 The time series for the wave height at the left tank wall for the first mode with $\epsilon = .07$ and $\delta = \frac{1}{2}$.

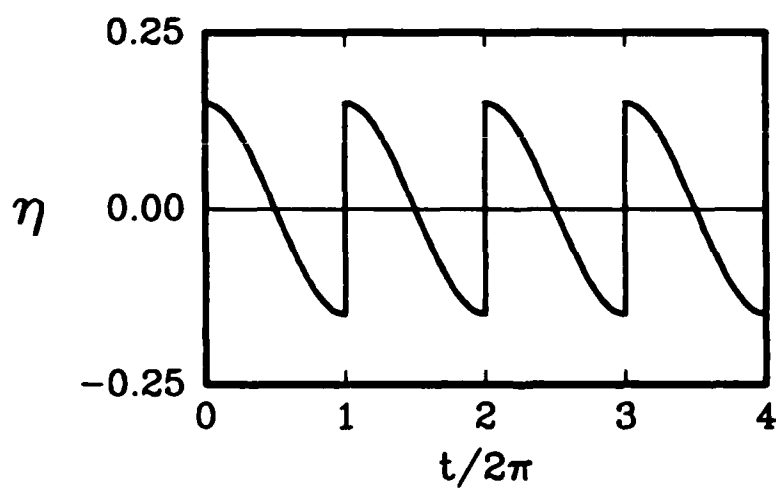


Figure 2.8 The time series of the wave height for Chester's discontinuous solution of the forced shallow water equations.

Although these singularities appear to be ominous they too are of higher order. The first singularity, $\sigma_3 = 2\sigma_1$ will not arise in the expansion until fifth order, at least, which renders it inconsequential. Also the other two singularities above will arise at the fifth or higher order. Presumably a proper modification of the expansion could be constructed (Mack [10] has done this for the critical depths arising in the circular standing wave problem, and Vanden-Broeck [17] has done this for the critical points arising in the capillary standing wave problem), but it is unlikely that the contribution to the overall solution in this case will be noticeable.

In light of these facts, the expansion of Tadjbakhsh and Keller will be valid, to the order given, for *all* depths, but only for a limited range of amplitudes, $\epsilon < \epsilon_m$.

It is worth noting that the problem for elliptic standing waves in the presence of a forcing function, where the forcing function is near the fundamental natural frequency, has been studied by Moisieiev [12], Faltinsen[7], and Lou. et al. [9]. The solutions are obviously similar to the eigenfunctions discussed here, but the important result is the relationship between the amplitude of the forcing function and the response amplitude. Moisieiev showed that, when the forcing frequency is near the linear resonant frequency, the response amplitude $\epsilon = O(\theta^{1/3})$ where θ is the amplitude of the forcing function. This means that the nature of the nonlinearity of the governing partial differential equation and boundary conditions (the operator) is *cubic* in the neighborhood of the bifurcation points. It will become clear in the analysis in Section 4 that the nature of the nonlinearity becomes *quadratic* when $\epsilon = O(\delta^2)$, and when $\epsilon \gg \delta^2$ the nonlinearity remains quadratic. Therefore this operator has the interesting property that the nature of the nonlinearity changes as the amplitude of the response increases. These conjectures are based on the interesting, and useful, theory of *imperfect bifurcation* [13], and singular perturbation of bifurcations [11], proposed by B. Matkowsky and E. Reiss. In that work, they propose a method for determining the degree of the nonlinearity of operators in the neighborhood of singularities (such as bifurcation points). This

information is then used to obtain the proper expansion parameter for the analysis of the imperfect bifurcation problem (a forcing function qualifies as an imperfection).

2.3 The Travelling Hydraulic Jump

The other theory proposed for waves in rectangular basins is Chesters [2,3] "shallow water theory". This theory is derived by taking the limit as $\delta \rightarrow 0$ with fixed, although small, amplitude. To proceed the equations (1.1)-(1.4) are scaled in the manner described earlier except ϕ and η are now independent of ϵ . The forcing terms are retained and their role in the existence of periodic solutions in this region of the $\delta - \epsilon$ plane will be elaborated.

In the limit as $\delta \rightarrow 0$ the Laplace equation in conjunction with the bottom boundary condition gives

$$\phi = \phi_0 + \Omega xy \delta^2 - \delta^2 \frac{(1+y)^2}{2} \frac{\partial^2 \phi_0}{\partial x^2} + \dots \quad (2.23)$$

where ϕ_0 is a function of x and t only. Substituting this expression into the free surface boundary conditions and neglecting terms of $O(\delta^2)$ and higher results in

$$\omega \frac{\partial \eta}{\partial t} + \frac{\partial \phi_0}{\partial x} \frac{\partial \eta}{\partial x} + (1 + \eta) \frac{\partial^2 \phi_0}{\partial x^2} = 0 \quad (2.24)$$

$$\omega \frac{\partial \phi_0}{\partial t} + \frac{1}{2} \left(\frac{\partial \phi_0}{\partial x} \right)^2 + \eta + \theta x = 0 \quad (2.25)$$

But the substitution $u = \partial \phi_0 / \partial x$ results in the common form of the shallow water equations

$$\omega \frac{\partial \eta}{\partial t} + u \frac{\partial \eta}{\partial x} + (1 + \eta) \frac{\partial u}{\partial x} = 0 \quad (2.26)$$

$$\omega \frac{\partial u}{\partial t} + u \frac{\partial u}{\partial x} + \frac{\partial \eta}{\partial x} = -\theta \quad (2.27)$$

with boundary conditions $u(\pm \frac{1}{2}, t) = 0$. This formulation, and the subsequent analysis, differs somewhat from that of Chester but the essentials are the same. The forcing function is taken to have the form $\theta = \epsilon^2 \cos t$. The amplitude of the forcing function is taken proportional to the response amplitude *squared*. Solutions are sought in the neighborhood of resonance and the nonlinearity and forcing function must balance in order to obtain a periodic solution. This suggests that the response in the neighborhood of resonance is of $O(|\theta|^{1/2})$. It also suggests that the nonlinearity of the operator is quadratic in the neighborhood of the linear eigenvalues. This is to be contrasted with the result when the operator was elliptic. The governing equations are now hyperbolic as well. Therefore, as the amplitude of the wave increases the governing equations and boundary conditions *change type* from elliptic to hyperbolic.

To obtain a formal solution of this problem in the limit as ϵ tends to zero, a power series solution in ϵ is sought

$$\omega = \omega_0 + \epsilon \omega_1 + \dots \quad (2.28a)$$

$$u = \epsilon u_1 + \epsilon^2 u_2 + \dots \quad (2.28b)$$

$$\eta = \epsilon \eta_1 + \epsilon^2 \eta_2 + \dots \quad (2.28c)$$

Substituting and equating terms proportional to like powers of ϵ to zero results in a sequence of inhomogeneous wave equations. Combining the two first order equations results in a homogeneous wave equation for u_1 ,

$$\square u_1 = 0 \quad (2.29)$$

where \square is the D'Alembertian,

$$\square \equiv \omega_0^2 \frac{\partial^2}{\partial t^2} - \frac{\partial^2}{\partial x^2} \quad (2.30)$$

with homogeneous boundary conditions. Retaining the mode number as arbitrary, the general solution is

$$u_1(x, t) = f(\xi) - f(\chi) \quad (2.31)$$

where $\xi = t + \alpha_m \bar{x}$ and $\chi = t - \alpha_m \bar{x}$, and $\omega_0 = \alpha_m = m\pi$. The wave height has a solution,

$$\eta_1(x, t) = -f(\xi) - f(\chi) \quad (2.32)$$

The function f is unknown at this order. It will be found by imposing the solvability condition at the next order. The second order equations are

$$\omega_0 \frac{\partial \eta_2}{\partial t} + \frac{\partial u_2}{\partial x} + \omega_1 \frac{\partial \eta_1}{\partial t} + u_1 \frac{\partial \eta_1}{\partial x} + \eta_1 \frac{\partial u_1}{\partial x} = 0 \quad (2.33)$$

$$\omega_0 \frac{\partial u_2}{\partial t} + \frac{\partial \eta_2}{\partial x} + \omega_1 \frac{\partial u_1}{\partial t} + u_1 \frac{\partial u_1}{\partial x} + \cos t = 0 \quad (2.34)$$

which can be combined to form an inhomogeneous wave equation for u_2 . After substituting the first order result into the right hand side, the result is

$$\begin{aligned} \square u_2 = & -2\alpha_m \omega_1 [f''(\xi) - f''(\chi)] - 3\alpha_m^2 [(f(\xi)f'(\xi))' - (f(\chi)f'(\chi))'] \\ & - \alpha_m^2 [f(\xi)f''(\chi) - f(\chi)f''(\xi)] + \alpha_m \sin\left(\frac{\xi + \chi}{2}\right) \end{aligned} \quad (2.35)$$

There is a solution to (2.35) if and only if the right hand side satisfies a Fredholm alternative. The necessary Fredholm alternative for the inhomogeneous wave equation is given in Appendix III. Application of this results in an ordinary differential equation for f ,

$$4\alpha_m^2 \omega_1 f''(\chi) + 6\alpha_m^3 (f(\chi)f'(\chi))' + 4\alpha_m \cos\left(\frac{\chi}{2}\right) = 0 \quad (2.36)$$

which may be integrated twice to yield,

$$f^2(\chi) + \frac{4\omega_1}{3\alpha_m} f(\chi) - \frac{16}{3\alpha_m^2} \cos\left(\frac{\chi}{2}\right) - c^2 = 0 \quad (2.37)$$

where $c^2 = \int_0^{2\alpha_m} f^2(x) dx$. It is interesting to note that if the forcing function were absent in (2.37) the solution would be $f(\chi) = \text{constant}$, but the constant would have to be zero to satisfy mass conservation. This shows that *there are no periodic solutions bifurcating from the state of rest for the shallow water equations (2.26) and (2.27) when the forcing function is absent*. In fact, Keller and Ting [8] have rigorously proved that for any set of quasilinear first order set of hyperbolic equations with two unknowns, the solutions become singular in finite time. In other words, the shock wave solutions are not eigenfunctions, they are states of degeneracy of the eigenfunctions.

However with the introduction of the forcing function periodic, albeit discontinuous, solutions may be found. With non-zero forcing function (2.37) has the following solution for the first mode,

$$f(\chi) = -\frac{2\omega_1}{3\pi} \pm \frac{4}{\pi} \sqrt{\frac{2}{3}} \sqrt{b^2 + \cos^2 \frac{\chi}{4}} \quad (2.38)$$

where

$$b^2 = \frac{3\pi^2}{32} \left\{ c^2 + \frac{4\omega_1^2}{9\pi^2} - \frac{16}{3\pi^2} \right\} \quad (2.39)$$

However, for mass conservation $f(\chi)$ must satisfy

$$\int_0^{2\pi} f(\chi) d\chi = 0 \quad (2.40a)$$

or

$$\omega_1 \pm \frac{12}{\pi} \sqrt{\frac{2}{3}(1+b^2)} \int_0^{\pi/2} \sqrt{1 - \kappa^2 \sin^2 x} dx = 0 \quad (2.40b)$$

where $\kappa^2 = (1+b^2)^{-1}$. (2.40b) contains an elliptic integral of the second kind with modulus κ which has a real solution for $0 \leq \kappa^2 \leq 1$ only. Therefore there are no continuous solutions for

$$|\omega_1| < \frac{12}{\pi} \sqrt{\frac{2}{3}} \quad (2.41)$$

But this is in fact the region of interest; the neighborhood of resonance. However, as shown by Chester, periodic *discontinuous* solutions can be found which satisfy (2.40). There are an infinity of discontinuous solutions which may be constructed, using the two solutions (2.38), which satisfy (2.40). However, as pointed out by Chester, when $b^2 \neq 0$ such solutions would include shocks of rarefaction type, which are non-physical. One can also use an energy argument requiring u and η to increase across the shock. Elaboration on these arguments are given in Chester [2], and Collins [5], in his more general study of nonlinear wave equations, constructs other arguments for finding unique discontinuous solutions based on an "entropy" argument as well as looking for discontinuous solutions as limits of solutions with small viscosity.

Therefore, taking $b^2 = 0$, the result is the following family of discontinuous solutions,

$$f(\chi) = \frac{4}{\pi} \sqrt{\frac{2}{3}} \left[-\frac{\omega_1}{2\sqrt{6}} + \cos \frac{\chi}{4} \right] \quad (2.42)$$

where

$$\sin^{-1} \left[-\frac{\pi\omega_1}{4\sqrt{6}} \right] < \frac{\chi}{4} < \pi + \sin^{-1} \left[-\frac{\pi\omega_1}{4\sqrt{6}} \right] \quad (2.43)$$

for $-1 \leq -\frac{\pi\omega_1}{4\sqrt{6}} \leq 1$. Substituting this expression into (2.32) results in the first order wave height,

$$\eta_1 = \frac{4\omega_1}{3\pi} - \frac{4}{\pi} \sqrt{\frac{2}{3}} \left(\cos \frac{\xi}{4} + \cos \frac{\chi}{4} \right) \quad (2.44)$$

In Figure 2.8 this expression is plotted for fixed x (the left tank wall) as a function of time. The forcing function is equal to the first natural frequency ($\omega_1 = 0$). Since the depth has been ruled out through the limit process, all one can say is that the depth is "very shallow". Chester [2] has plotted the result for other forcing frequencies by varying ω_1 . They are similar to Figure 2.8 but the solutions become continuous as ω_1 exceeds the resonance region, given by (2.41).

In the next section these theories will be compared with an experimental study.

3. Experimental Study of Elliptic Standing Waves and Hydraulic Jumps

3.1 Introduction

An experimental study was undertaken with the primary goal of exploring the nature of the surface waves between the two regions discussed in the previous section. In addition some previously unrecognized facets of elliptic standing waves and travelling hydraulic were illuminated. The experimental observations made for the neighborhood of the $\delta - \epsilon$ plane between elliptic standing waves and shocks will be discussed in detail in Section 5. It is the purpose here to describe some experimental observations obtained for the theoretical regions discussed in Section 2.

The regimes observed in the experiment are broken down in Figure 3.1 where a rough diagram of the waves observed for various combinations of ϵ and δ are plotted. The points near the diagonal are the observed values of ϵ , for fixed δ , where standing waves, of any variety, were observed to break down. Curves of $\epsilon = \delta$, $\epsilon = \delta^2$ as well as $\epsilon = (\pi\delta)^2$ are superimposed on the diagram. It is seen that the breakdown of standing waves occurs at $\epsilon \sim \delta$ or equally well $\epsilon \sim (\pi\delta)^2$. There is then an intermediate region where compound waves are observed, which will be discussed in Section 5, and then when $\epsilon > \text{about } \frac{1}{2}$ and $\delta < \text{about } .15$ the travelling hydraulic jump is observed exclusively. Although the travelling jump is three dimensionally unsteady in a strict sense, in the large it is essentially two dimensional and in fact very stable. Once the hydraulic jump is formed, regardless of how much the amplitude of the tank motion is increased, the jump is maintained with the strength increasing slightly with increasing tank motion. The curved labelled line in the figure is an extrapolation of the result of Schwartz and Whitney [14]. They showed that for fluid of infinite depth (the purest of elliptic standing waves) the maximum height of a stable waveform was reached when $H/2a \sim .2$. In terms of ϵ and δ this is $\epsilon \sim .2/\delta$ which is superimposed on the figure. This gives an upper bound for elliptic standing waves, and may be an upper bound for all types of irrotational waves appearing in rectangular vessels. The intersection of this

curve with the $\epsilon = \delta^2$ curve at $\delta \sim .6$ suggests that for $\delta > .6$ the only class of existing waves are the elliptic standing waves.

The experimental arrangement which was constructed in order to observe these waves is now described and then the results will be discussed.

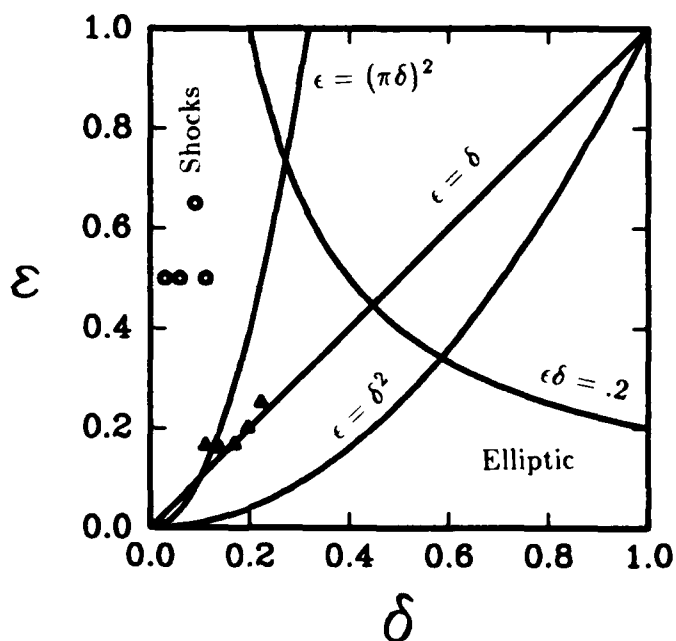


Figure 3.1 A diagram of the δ - ϵ plane which shows approximately where the various classes of waves were observed to exist. The triangles represent the values of ϵ for fixed δ where standing waves were no longer observed, and the circles represent the lowest values of ϵ for fixed δ where a travelling hydraulic jump was observed.

3.2 Experimental Setup

The experimental setup is depicted in Figures 3.2 and 3.3. It was constructed and setup at the *MIPAC Research Facility* at the *Mathematics Research Center*. The tank, constructed of $\frac{1}{4}$ " thick plexiglass, has the following dimensions: tank length, $2a = 18$ ", tank breadth = 3 ", and the tank height = 15 ". Although the tank height was 18 ", the fill depth was limited to about 6 " due to the large inertial force imposed by the fluid on the driving mechanism causing perturbations to the otherwise strictly sinusoidal forcing function. The natural frequencies in Hz of the first five (two dimensional) modes, as a function of the dimensionless depth δ , for a vessel of this dimension is shown in Figure 3.4. It is important to note, however, that in a rigid tank undergoing forced harmonic oscillation only *odd* modes may be excited. In fact, it appears that the only way to excite even modes is to move the endwalls harmonically. This is how Taylor [16] excited standing waves in his study of the limiting configuration of standing waves in deep water. In his case the mode studied and depicted in photos in his paper was the $m=2$ mode. Due to the rigid walls only odd modes are elicited in this study.

A steel shaft, rigidly bolted to the bottom center of the tank and mounted in rotary bearings on a wooden support stand, acts as the pivot for the roll motion of the tank. A driving arm, attached perpendicular to the shaft, is connected to the driving mechanism, which oscillates vertically. With this arrangement the vertical oscillation of the driving mechanism imparts an angular rotation to the tank, i.e. roll motion. The driving mechanism is a Brüel & Kjær Vibration Exciter Type 4808. It is an electromagnetic vibration exciter much like a loudspeaker, where the movement is produced by a current passing through a coil in a magnetic field. The amplitude of the excitation is varied by controlling the current. The harmonic output, to the driving mechanism, is created in and controlled by the *HP 5451C Fourier Analyzer* shown in Figure 3.3.

Figure 3.2 The apparatus used to study the waves in a rectangular basin. The black object in the background is a vertical oscillator which provides the forcing function. The electronics to the left pre-process the wave height time series for input into the Fourier analyzer.

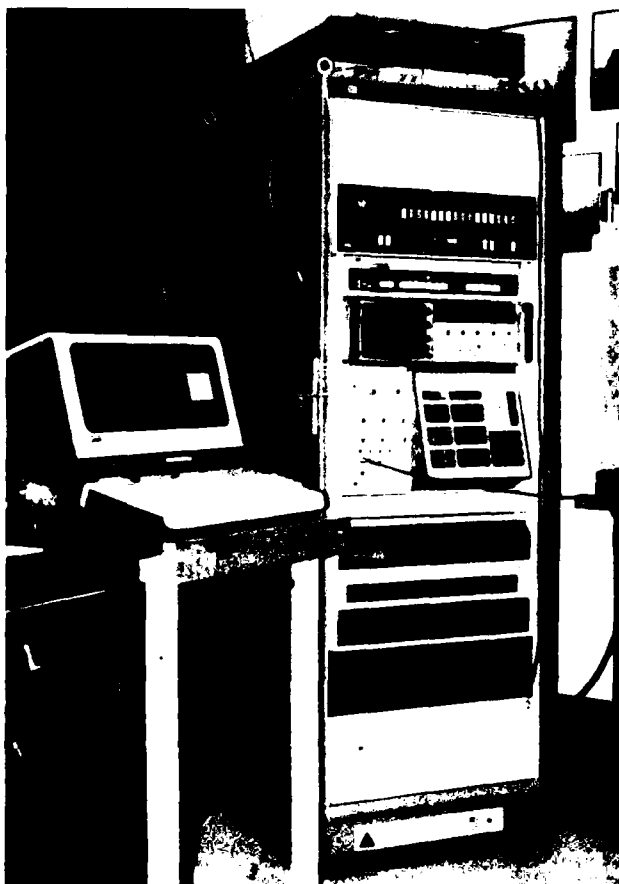
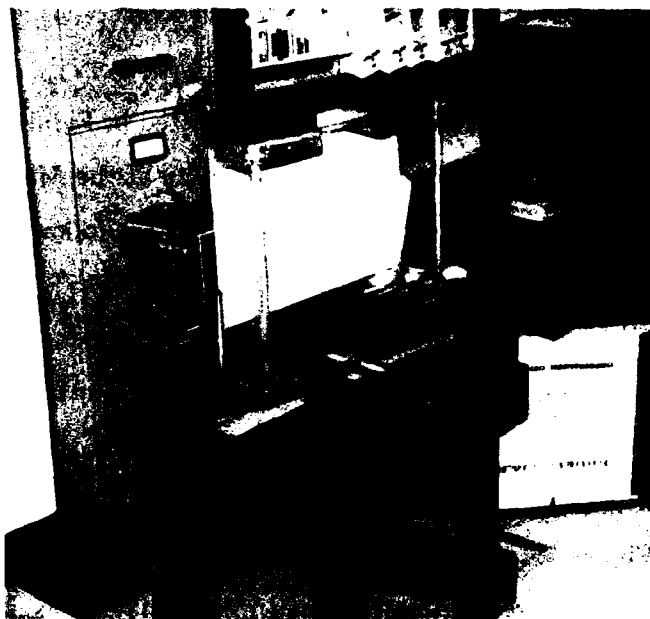


Figure 3.3 The HP Fourier analyzer which drives the oscillator; records and analyzes the experimental data.

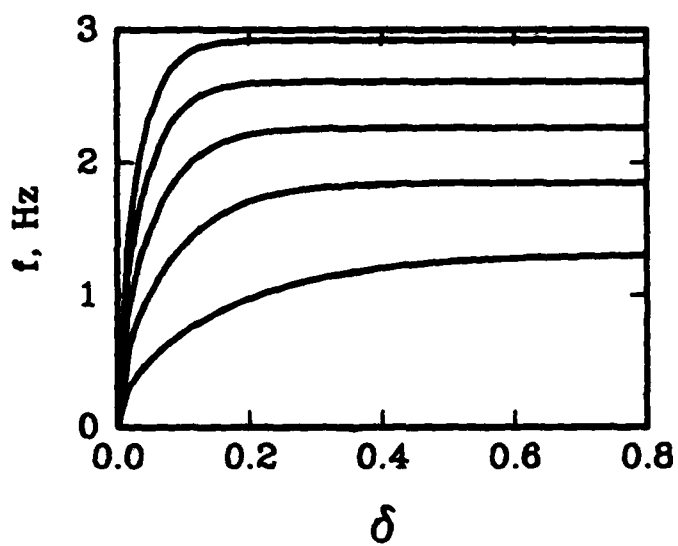


Figure 3.4 The linear natural frequencies corresponding to the first five modes for the experimental tank as a function of dimensionless fill depth δ .

The *HP 5451C Fourier Analyzer* is a programmable minicomputer which creates, inputs, outputs, and analyzes time series. Fourier analysis programs such as the (a) forward and inverse Fourier transform, (b) power and cross-power spectrum, (c) transfer function, (d) coherence function, (e) convolution, (f) auto and cross correlation, (h) ensemble averaging, etc., are built in and can be performed through keyboard commands without special software. In addition, the analyzer can be programmed to run the experiment and input and analyze the various sensory measurements such as the local wave height and the tank rotary displacement. In this experiment the Fourier analyzer is programmed to do the following. It creates, given the desired frequency or frequencies, and outputs a time series to the exciter. The amplitude of the exciter is controlled in real time and can be continuously varied. The Fourier analyzer then receives and analyzes on command the time series of the wave height and or tank displacement. A hard wired external plotter is used to plot the results, and an hard disk is used for storage of the programs and data blocks.

The wave height is measured using a taut-wire capacitive wave gauge mounted one inch from the left tank wall. The electronics, which convert the changing capacitance, produced by the water riding up and down the wire, to a changing voltage, which is then input into the Fourier analyzer, is mounted to the left of the tank in Figure 3.2. The Fourier analyzer plots the signal and computes the Fourier transform to deduce the frequency content.

3.3 Experimental Observations

In the experiment the wave forms are elicited by forcing the tank to oscillate. Therefore there is not complete congruence between the solutions observed and the bifurcation analysis of, for example, Tadjbakhsh and Keller. However, when the forcing frequency is near resonance, the solutions of the forced problem should be very near those of the bifurcation analysis. Therefore the forcing frequency will be near resonance unless otherwise noted. An experimental setup of this kind is dependent on five dimensionless parameters; γ and d which specify the point of rotation (however in this experiment these are fixed at $\gamma = \frac{\pi}{2}$ and $d = \delta$), δ the fluid depth, and ω and ϑ the frequency and amplitude of the forcing function. The amplitude of the response, ϵ , is also a parameter, but it is posited that there is a functional relationship between ϵ and ϑ . Therefore for a particular "run", once the depth is fixed the only parameters are the frequency ω (actually f will be used where $f = \omega/2\pi$) and amplitude ϑ of the forcing function.

Observations of elliptic standing waves will now be discussed. As pointed out in Section 2 these solutions occur at all depths but for only a limited range of amplitude. Therefore consider the fill depth $\delta = .2$. Here the relevant natural frequencies are $f_1 = 1.04Hz$, $f_3 = 2.22Hz$, and $f_5 = 2.93Hz$. In Figures 3.5, 3.6, and 3.7 photos of the 1, 3, and 5 mode respectively are shown. In each case the forcing function was set equal to the linear natural frequency. These figures may be compared to the result of the theory of Tadjbakhsh & Keller shown in Figures 2.4 and 2.6. The results are similar. These figures are in fact typical of the elliptic variety of standing waves. It is interesting that the waves of this type *look elliptic*. The body of fluid moves uniformly as if every particle were aware of every other particles motion. A striking contrast to hyperbolic waves.

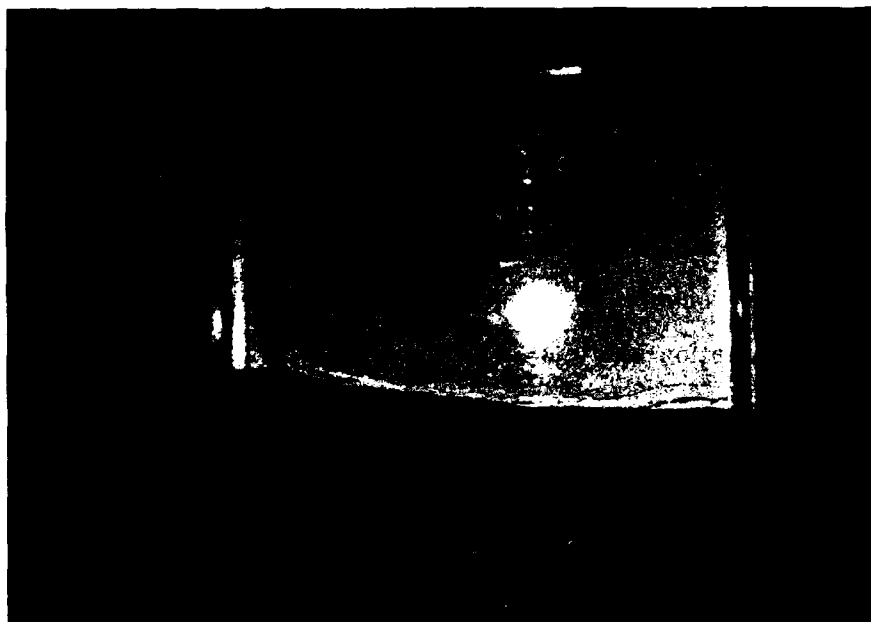


Figure 3.5 A classical mode 1 elliptic standing wave, where $\delta = .20$, $f = f_1 = 1.04$ Hz.



Figure 3.6 A mode 3 elliptic standing wave, showing signs of a three dimensional instability at the peaks, with $\delta = .2$ and $f = f_3 = 2.22$ Hz.

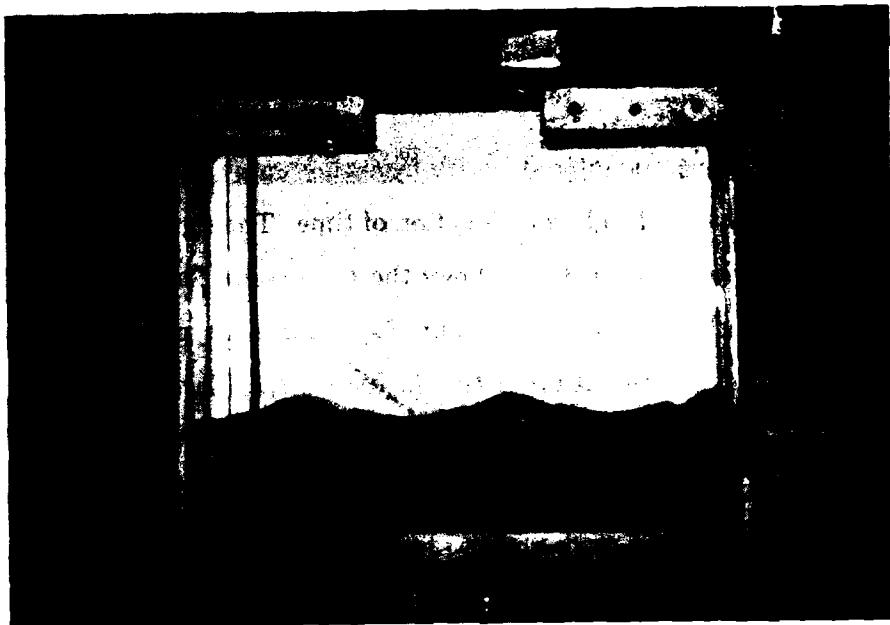


Figure 3.7 A mode 5 elliptic standing wave, with $\delta = .2$ and $f = f_5 = 2.93$ Hz.

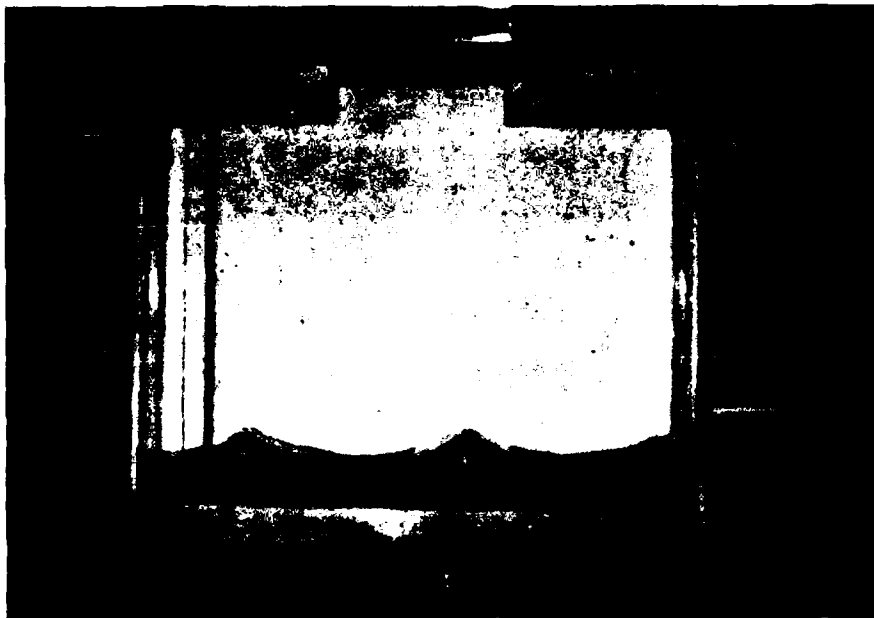


Figure 3.9a With $\delta = .077$ and $f = f_5 = 2.68$ a mode 5 elliptic standing wave occurs.

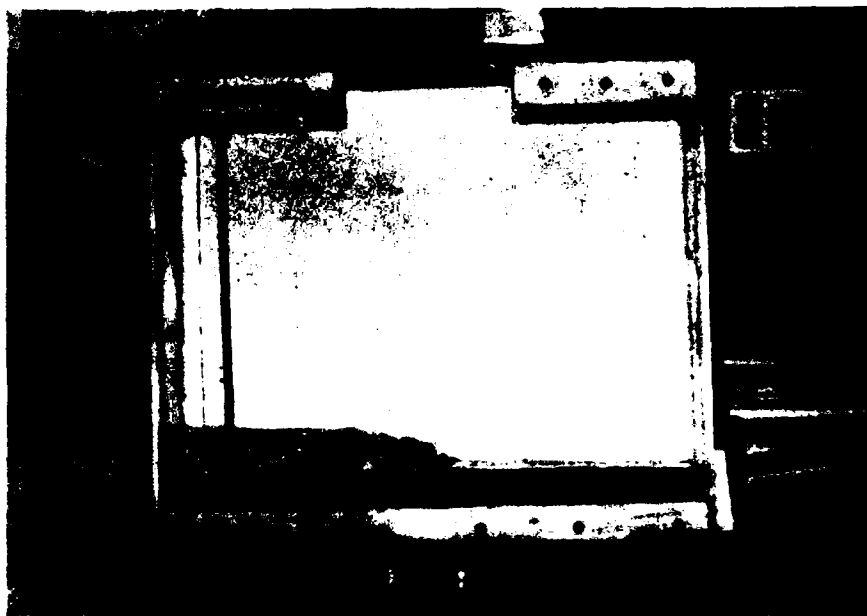


Figure 3.9b However, at the same depth $\delta = .077$, but with a lower frequency $f = f_1 = .64$ and sufficiently large amplitude, a travelling hydraulic jump is formed.

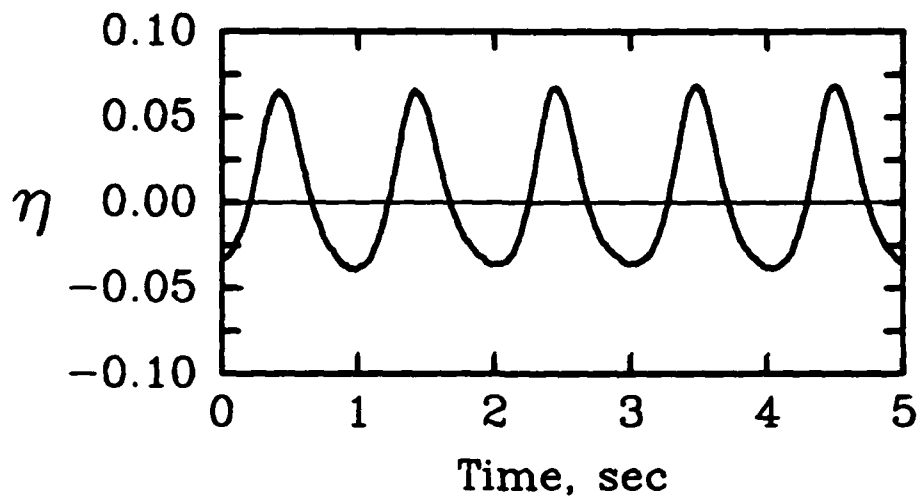


Figure 3.10a The time series for the wave height (one inch from the left tank wall) when $\delta = .20$ and $f = f_1 = .9702$. This is a typical result for the elliptic standing wave and closely resembles the theoretical result shown in Figure 2.7.

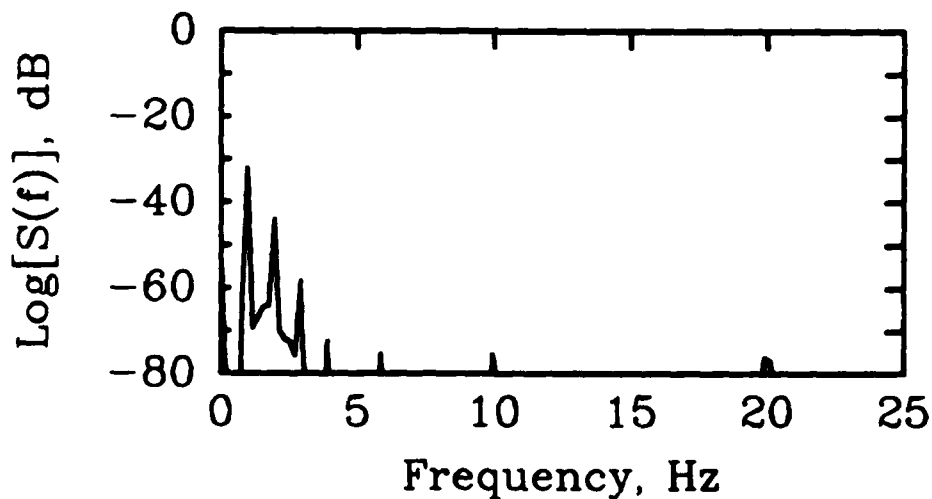


Figure 3.10b The Log magnitude of the Fourier transform of the time series in Figure 3.10a. It is essentially a discrete spectrum with the minor peak at the forcing function and the 2nd and 3rd peaks at twice and three times the forcing function, suggesting that the three term expansion of Tajdbakhsh and Keller is sufficient to describe this wave temporally.

The time series for the wave height shows this as well. Figure 3.11a shows the time series for the "deep water jump" when $\delta = .104$ and $f = f_1$. Although the time series is "almost discontinuous", and periodic "in the large" there is some irregularity due to the small amount of dispersion present. The Log of the Fourier transform of this wave height is given in Figure 3.11b. It shows the richness of the harmonics present. The time series for the "shallow water jump" is depicted in Figure 3.12a. Here the time series is more regular and the "almost discontinuous" nature of the wave height is obvious. The presence of dissipation prevents the solution from becoming truly discontinuous but nevertheless the experimental time series is approaching the theoretical prediction of Chesters shown in Figure 2.8. The Log of the Fourier transform for this time series is shown in Figure 3.12b. The explosion of harmonics over that occurring for the standing wave problem is obvious. But this is to be expected from a function which is almost discontinuous.

In the next section a theory for the "missing link" between elliptic standing waves and the hydraulic jump is proposed.

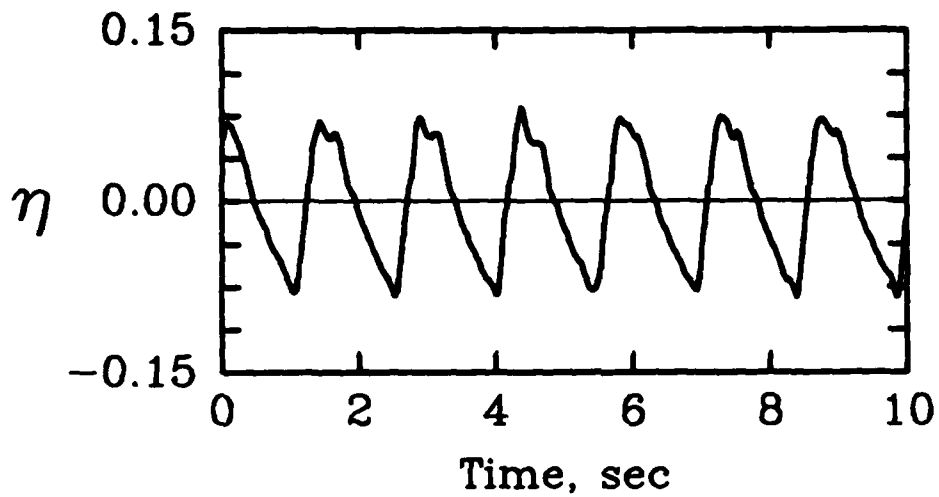


Figure 3.11a Time series for a "deep water" travelling hydraulic jump where $\delta = .105$ and $f = f_1 = .74$. At this depth there remains enough dispersion to produce an irregular travelling jump.

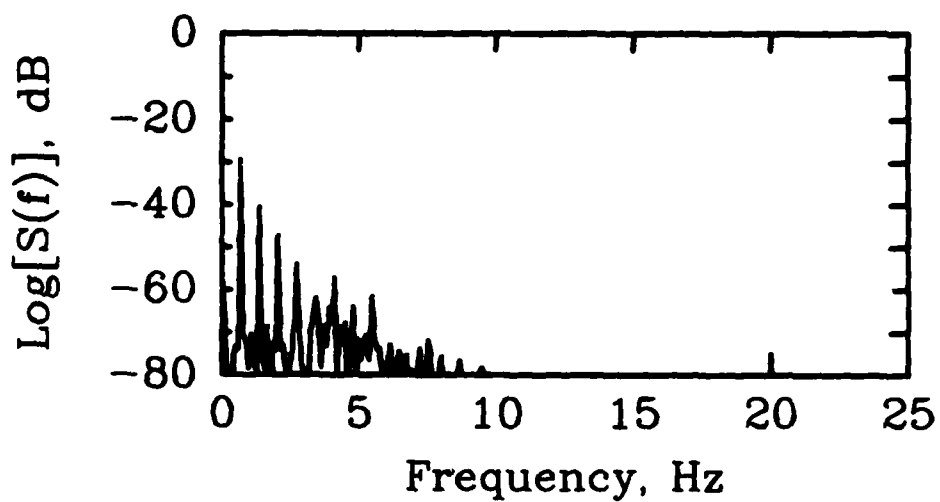


Figure 3.11b Log magnitude of the Fourier transform of the time series in Figure 3.11a. Due to the "almost discontinuous" nature of the time series the spectrum is rich.

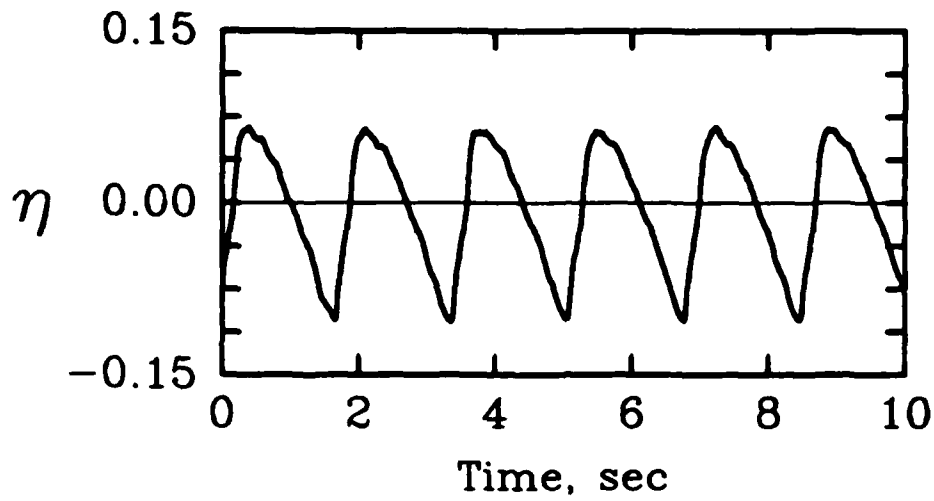


Figure 3.12a Time series for a "shallow water" travelling hydraulic jump where $\delta = .077$ and $f = f_1 = .64$. Here the function is more regular and begins to resemble the shallow water solution of Chester in Figure 2.8.

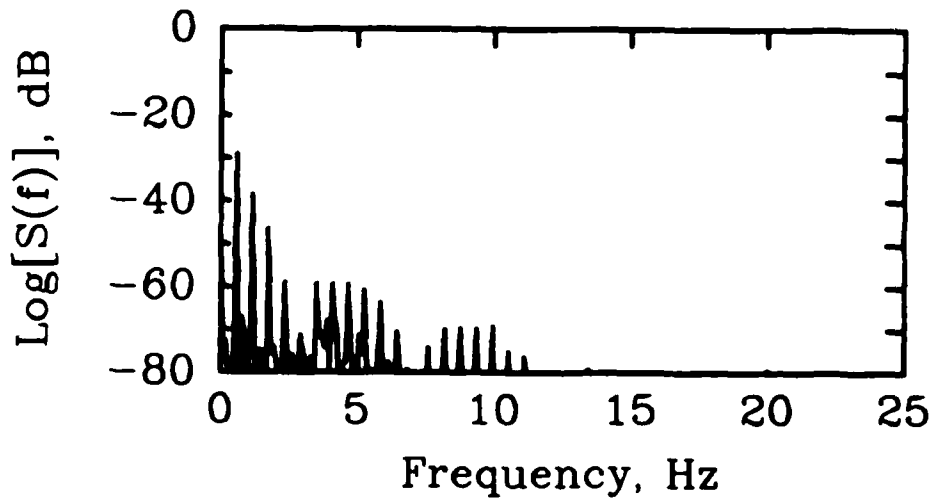


Figure 3.12b Log magnitude of the Fourier transform of the time series in Figure 3.11b. The spectrum is again rich due to the nature of the hydraulic jump.

4. Theory - II: Cnoidal Standing Waves

The solution for finite amplitude standing waves in fluid of arbitrary but finite depth was first derived by Tajdbakhsh and Keller [15] and extended to arbitrary mode number in Section 2. It was also shown in Section 2 that this solution is not uniformly valid in the amplitude. When $\epsilon = O(\delta^2)$ there is a spillover of the higher harmonics onto the zeroth order solution violating the tenet of the expansion. This spillover is in fact the first sign of the change of type of the standing wave. The amplitude (ϵ) is beginning to get large enough to challenge the role of the dispersion (δ^2). When $\epsilon \ll \delta^2$ the dispersion dominates and the solution is the well-behaved elliptic standing wave, and when $\epsilon \gg \delta^2$ the dispersion can no longer check the coalescence of the harmonics and they run together as a hydraulic jump.

There is however an intermediate region where the dispersion and the amplitude are in harmony, i.e. $\epsilon = O(\delta^2)$. A theory for the wave forms in this region is proposed in this section. In order for the relation $\epsilon = O(\delta^2)$ to hold δ must be sufficiently small. Therefore an asymptotic solution is sought with the simultaneous limit $\epsilon \rightarrow 0$ and $\delta \rightarrow 0$, but with the requirement that ϵ/δ^2 remain constant. This is done by taking the relationship $\delta = \sqrt{\tau\epsilon}$ where $\tau = O(1)$ and carries the sign of ϵ .

The governing equations and boundary conditions are the same as (2.1)-(2.3) but with the substitution $\delta = \sqrt{\tau\epsilon}$,

$$\tau\epsilon \frac{\partial^2 \phi}{\partial x^2} + \frac{\partial^2 \phi}{\partial y^2} = 0 \quad \text{in} \quad -\frac{1}{2} \leq x \leq \frac{1}{2}, -1 \leq y \leq \epsilon\eta \quad (4.1)$$

$$\frac{\partial \phi}{\partial x} = 0 \quad \text{at} \quad x = \pm \frac{1}{2} \quad (4.2a)$$

$$\frac{\partial \phi}{\partial y} = 0 \quad \text{at} \quad y = -1 \quad (4.2b)$$

$$\tau\epsilon\omega \frac{\partial \eta}{\partial t} + \tau\epsilon^2 \frac{\partial \eta}{\partial x} \frac{\partial \phi}{\partial x} - \frac{\partial \phi}{\partial y} = 0 \quad \text{on} \quad y = \epsilon\eta(x, t) \quad (4.3)$$

$$\omega \frac{\partial \phi}{\partial t} + \epsilon \frac{1}{2} \left(\frac{\partial \phi}{\partial x} \right)^2 + \frac{1}{2\tau} \left(\frac{\partial \phi}{\partial y} \right)^2 + \eta = 0 \quad \text{on } y = \epsilon \eta(x, t) \quad (4.4)$$

With ϵ as the only small parameter appearing, a power series solution in ϵ is sought,

$$\omega = \omega_0 + \epsilon \omega_1 + \epsilon^2 \omega_2 + \dots \quad (4.5)$$

$$\eta = \eta_0 + \epsilon \eta_1 + \epsilon^2 \eta_2 + \dots \quad (4.6)$$

$$\phi = \phi_0 + \epsilon \phi_1 + \epsilon^2 \phi_2 \dots \quad (4.7)$$

These expressions are substituted into the governing equations and boundary conditions, the free surface boundary conditions are expanded in a Taylor series about the still water level, and terms proportional to like powers of ϵ are set to zero resulting in a sequence of boundary value problems. The Laplace equation gives,

$$\phi_0 = \psi_0(x, t) \quad (4.8)$$

$$\phi_1 = \psi_1(x, t) - \frac{\tau}{2} (1 + y)^2 \frac{\partial^2 \psi_0}{\partial x^2} \quad (4.9)$$

$$\phi_2 = \psi_2(x, t) - \frac{\tau}{2} (1 + y)^2 \frac{\partial^2 \psi_1}{\partial x^2} + \frac{\tau^2}{24} (1 + y)^4 \frac{\partial^4 \psi_0}{\partial x^4} \quad (4.10)$$

etc.. These may then be substituted into the free surface boundary conditions. The zeroth order problem is then

$$\eta_0 + \omega_0 \frac{\partial \psi_0}{\partial t} = 0 \quad (4.11)$$

$$\omega_0 \frac{\partial \eta_0}{\partial t} - \frac{\partial^2 \psi_0}{\partial x^2} = 0 \quad (4.12)$$

and the first order problem is

$$\eta_1 + \omega_0 \frac{\partial \psi_1}{\partial t} - \frac{\omega_0 \tau}{2} \frac{\partial^3 \psi_0}{\partial x^2 \partial t} + \omega_1 \frac{\partial \psi_0}{\partial t} + \frac{1}{2} \left(\frac{\partial \psi_0}{\partial x} \right)^2 = 0 \quad (4.13)$$

$$\omega_0 \frac{\partial \eta_1}{\partial t} + \frac{\partial^2 \psi_1}{\partial x^2} - \frac{\tau}{6} \frac{\partial^4 \psi_0}{\partial x^4} + \omega_1 \frac{\partial \eta_0}{\partial t} + \frac{\partial \eta_0}{\partial x} \frac{\partial \psi_0}{\partial x} + \eta_0 \frac{\partial^2 \psi_0}{\partial x^2} = 0 \quad (4.14)$$

and this may be continued to higher order. Here the solution will be carried through the first order.

Combining (4.11) and (4.12) the zeroth order problem is a homogeneous wave equation,

$$\square \psi_0 = 0 \quad (4.15)$$

where \square is the D'Alembertian,

$$\square \equiv \omega_0^2 \frac{\partial^2}{\partial t^2} - \frac{\partial^2}{\partial x^2} \quad (4.16)$$

with the additional requirement that $\partial \psi_0 / \partial x$ vanish on the vertical boundary $x = \pm \frac{1}{2}$. (4.15) and the wall boundary condition have the general solution

$$\omega_0 = \alpha_m \quad (4.17)$$

$$\psi_0 = f(\xi) + f(\chi) \quad (4.18)$$

where $\xi = t + \alpha_m \bar{x}$, $\chi = t - \alpha_m \bar{x}$, $\alpha_m = m\pi$, and $\bar{x} = x + \frac{1}{2}$. With (4.11) the zeroth order wave height is found to be

$$\eta_0 = -\alpha_m [f'(\xi) + f'(\chi)] \quad (4.19)$$

The function $f(\xi)$ is, however, unknown at this order. The Fredholm solvability condition applied at the next order will result in an expression for $f(\xi)$.

The zeroth order result (4.17)-(4.18) are substituted into (4.13)-(4.14). The two equations are combined to form the following inhomogeneous wave equation for ψ_1 ,

$$\square \psi_1 = F_1(x, t) \quad (4.20)$$

where

$$\begin{aligned} F_1(x, t) = & \frac{\tau \alpha_m^4}{3} \{f''''(\xi) + f''''(\chi)\} - 2\alpha_m \omega_1 \{f''(\xi) + f''(\chi)\} \\ & - 3\alpha_m^3 \{f'(\xi)f''(\xi) + f'(\chi)f''(\chi)\} \\ & + \alpha_m^3 \{f''(\xi)f'(\chi) + f'(\xi)f''(\chi)\} \end{aligned} \quad (4.21)$$

(4.20) has a solution if and only if $F_1(x, t)$ satisfies,

$$\int_0^{2\alpha_m} F\left[\frac{\xi - \chi}{2\alpha_m}, \frac{\xi + \chi}{2}\right] d\xi = 0 \quad (4.22)$$

This is a variant of the Fredholm alternative and is proved in Appendix III. Application of this requirement results in the following nonlinear ordinary differential equation for f ,

$$\frac{\tau\alpha_m^4}{3} f''''(\chi) - 2\alpha_m\omega_1 f''(\chi) - 2\alpha_m^3 f'(\chi) f''(\chi) = 0 \quad (4.23)$$

but defining $h(\chi) = -\alpha_m f'(\chi)$ and integrating the equation once,

$$\tau h''(\chi) - \frac{6\omega_1}{\alpha_m^3} h(\chi) + \frac{9}{2\alpha_m^2} h^2(\chi) - \frac{9}{4\alpha_m^3} I_1 = 0 \quad (4.24)$$

Conservation of mass requires $\int_0^{2\alpha_m} h(x) dx = 0$, therefore I_1 is a positive definite constant given by

$$I_1 = \int_0^{2\alpha_m} h^2(x) dx \quad (4.25)$$

It is important to note that the *nonlinearity* of the resulting expression for $h(\chi)$ is *quadratic*. This suggests that the nonlinearity of the operator is quadratic in that region of the $\delta - \epsilon$ plane where $\epsilon = 0(\delta^2)$ (and this may also be true for $\epsilon \gg \delta^2$). The operator for $\epsilon \ll \delta^2$ is *cubic* in the nonlinearity as discussed in Section 2.

The solution of (4.24) can be found in terms of Jacobian elliptic functions, i.e.,

$$h(\chi) = A + B \operatorname{cn}^2(\chi; \kappa) \quad (4.26)$$

when $w_1 = \frac{3}{2}\alpha_m A - \frac{2}{3}\tau\alpha_m^3(1 - 2\kappa^2)$, and

$$A = -\frac{4}{3}\alpha_m^2 \tau \left\{ \kappa^2 - 1 + \frac{1}{\pi} E(\pi; \kappa) \right\} \quad (4.27)$$

$$B = \frac{4}{3}\kappa^2 \tau \alpha_m^2 \quad (4.28)$$

and the constant I_1 is found to have the following expression,

$$I_1 = 2\alpha_m A^2 - \frac{8\omega_1}{3} A + \frac{8}{9}\tau\alpha_m^3 B(1 - \kappa^2) \quad (4.29)$$

The $\text{cn}(\chi; \kappa)$ is the family of cnoidal functions with modulus κ . Necessary details for this and the other Jacobian elliptic functions are given in Appendix IV. $f(\chi)$ is found by integrating $h(\chi)$

$$f(\chi) = -\frac{4}{3}\tau\alpha_m\kappa^2 Z(\chi; \kappa) + \text{constant} \quad (4.30)$$

where $Z(\chi; \kappa)$ is the Jacobian Zeta function. The constant is arbitrary and it is chosen for convenience to be zero to satisfy $\int_0^{2\alpha_m} f(\chi) d\chi = 0$. A complete description of the zeroth order solution may now be given,

$$\omega_0 = \alpha_m \quad (4.31)$$

$$\phi_0(x, t) = -\frac{4}{3}\tau\alpha_m\kappa^2 [Z(t + \alpha_m\bar{x}; \kappa) + Z(t - \alpha_m\bar{x}; \kappa)] \quad (4.32)$$

$$\begin{aligned} \eta_0(x, t) = & -\frac{8}{3}\alpha_m^2\tau[\kappa^2 - 1 + \frac{1}{\pi}E(\pi; \kappa)] \\ & + \frac{4}{3}\kappa^2\tau\alpha_m^2[\text{cn}^2(t + \alpha_m\bar{x}; \kappa) + \text{cn}^2(t - \alpha_m\bar{x}; \kappa)] \end{aligned} \quad (4.33)$$

and the first order correction to the frequency is found to be

$$\omega_1 = -2\tau\alpha_m^3 \left[\frac{1}{\pi}E(\pi; \kappa) - \frac{1}{3}(2 - \kappa^2) \right] \quad (4.34)$$

which is positive definite. Therefore the bifurcation is supercritical; i.e. the natural frequency increases with increasing amplitude. It is interesting to note that τ and α_m^2 usually appear together. Recalling that $\epsilon = \frac{1}{\tau}\delta^2$, it was found in the solution for elliptic standing waves that spillover occurs when $\epsilon = (\alpha_m\delta)^2$. In addition, as shown in Appendix IV equation (IV.6), the cnoidal function has a complete Fourier cosine series showing that when $\epsilon = 0(\delta^2)$ all the higher harmonics are present in the solution.

With $f(\chi)$ known, it may be substituted into the right hand side of (4.20) and upon integration the first order solution for ψ_1 is found to be

$$\psi_1 = -\frac{I_1}{2\alpha_m^2}(\xi + \chi) + \frac{\alpha_m}{4}[f(\xi)f'(\chi) + f(\chi)f'(\xi)] + [f_1(\xi) + f_1(\chi)] \quad (4.35)$$

and by combining with (4.9) the complete expression for the first order potential is

$$\begin{aligned}\phi_1 = & -\frac{I_1}{2\alpha_m^2}(\xi + \chi) + \frac{\alpha_m}{4}[f(\xi)f'(\chi) + f(\chi)f'(\xi)] + \frac{\tau}{2}\alpha_m(1+y)^2[h'(\xi) + h'(\chi)] \\ & + [f_1(\xi) + f_1(\chi)]\end{aligned}\quad (4.36)$$

and with (4.13) the first order wave height is

$$\begin{aligned}\eta_1 = & \frac{I_1}{2\alpha_m} + \frac{\omega_1}{\alpha_m}[h(\xi) + h(\chi)] - \frac{1}{2}h(\xi)h(\chi) - \frac{\alpha_m^2\tau}{2}[h''(\xi) + h''(\chi)] \\ & + \frac{\alpha_m}{4}[f(\xi)h'(\chi) + f(\chi)h'(\xi)] - \frac{1}{2}[h(\xi) - h(\chi)]^2 \\ & - \alpha_m[f_1'(\xi) + f_1'(\chi)]\end{aligned}\quad (4.37)$$

The function $f_1(\xi)$, as well as the second order correction to the frequency, may be found by imposing the Fredholm solvability condition to the second order problem.

The main result is that the zeroth order wave height is given by a family of left and right running cnoidal waves with parameter κ varying over $0 \leq \kappa^2 \leq 1$. The combination of the left running and right running waves forms a standing cnoidal wave. If $\kappa^2 = 1$, then $\text{cn}(\xi; 1) \rightarrow \text{sech}(\xi)$ which would then suggest that the waves would be a combination of a right and left running solitary wave. However, this is not the case since the solitary wave, due to the necessity of an infinitely long tail, will not satisfy the periodicity condition. In fact if it is required that the solution be periodic in time with period 2π then there is only one member of the κ family which will satisfy this. The $\text{cn}^2(\xi; \kappa)$ function is periodic with period $2K(\frac{\pi}{2}; \kappa)$, where $K(\frac{\pi}{2}; \kappa)$ is the complete elliptic integral of the first kind. Therefore the admissible value of $K(\frac{\pi}{2}; \kappa)$ is given by the root of the transcendental equation,

$$\pi - \int_0^{\frac{\pi}{2}} \frac{d\zeta}{\sqrt{1 - \kappa^2 \sin^2 \zeta}} = 0 \quad (4.38)$$

A numerical solution of this equation results in a value for κ^2 of $\kappa^2 \sim .9691$.

The second order frequency correction ω_2 and the function $f_1(\chi)$ may be found through application of the solvability condition on the second order problem. The second order problem has the form

$$\eta_2 + \omega_0 \frac{\partial \phi_1}{\partial t} + \omega_2 \frac{\partial \phi_0}{\partial t} + \frac{\partial \phi_0}{\partial x} \frac{\partial \phi_1}{\partial x} + \frac{1}{2\tau} \left(\frac{\partial \phi_1}{\partial y} \right)^2 + \omega_0 \eta_0 \frac{\partial^2 \phi_1}{\partial y \partial t} = 0 \quad (4.39)$$

and

$$\begin{aligned} \omega_0 \frac{\partial \eta_2}{\partial t} - \frac{1}{\tau} \frac{\partial \phi_3}{\partial y} + \omega_1 \frac{\partial \eta_1}{\partial t} + \omega_2 \frac{\partial \eta_0}{\partial t} + \frac{\partial \eta_0}{\partial x} \frac{\partial \phi_1}{\partial x} + \frac{\partial \eta_1}{\partial x} \frac{\partial \phi_0}{\partial x} \\ - \frac{\eta_0}{\tau} \frac{\partial^2 \phi_2}{\partial y^2} - \frac{\eta_1}{\tau} \frac{\partial^2 \phi_1}{\partial y^2} = 0 \end{aligned} \quad (4.40)$$

When these equations are combined and the solvability condition is applied, after some integration and algebraic manipulation the resulting differential equation for $f_1(\chi)$ is

$$\begin{aligned} \tau f_1'''(\chi) - \frac{6\omega_1}{\alpha_m^3} f_1'(\chi) + \frac{9}{2\alpha_m^2} h(\chi) f_1'(\chi) = \text{constant} \\ + \left\{ \frac{6\omega_2}{\alpha_m^4} + \frac{3I_1}{4\alpha_m^4} + \frac{4\tau d_1}{15\alpha_m} - \frac{57\omega_1^2}{5\alpha_m^5} \right\} h(\chi) - \frac{5\tau d_2}{2\alpha_m} h^2(\chi) - \frac{2\tau}{\alpha_m} h'(\chi) h'(\chi) \end{aligned} \quad (4.41)$$

where the numbers d_1 and d_2 are given in Appendix IV, and the integration constant is chosen such that the integral of $f_1(\chi)$ is zero. The equation is a linear differential equation with nonconstant coefficients which has the homogeneous solution $f_1' h(\chi) = \beta h(\chi)$ where β is an arbitrary constant. The inhomogeneous part must satisfy an additional solvability condition. After multiplication of (4.41) by $h(\chi)$ and integration from 0 to $2\alpha_m$ the left hand side is zero and the integral of the right hand side results in an expression for ω_2 ,

$$\omega_2 = -\frac{1}{8} I_1 - \frac{2}{45} d_1 \alpha_m^3 + \frac{57\omega_1^2}{30\alpha_m} + \frac{\tau \alpha_m^3}{12I_1} (5d_2 I_4 - 2I_5) \quad (4.42)$$

where the constants d_1 , d_2 , I_4 , and I_5 are given in Appendix IV. After substitution of this into (4.41) it can be shown that (4.41) has the general solution

$$f_1'(\chi) = A_1 + A_2 h(\chi) + \frac{4}{7\alpha_m} h^2(\chi) \quad (4.43)$$

The arbitrariness of A_1 is due to the integration constant in (4.41) and the arbitrariness of A_2 is due to the homogeneous solution of (4.41). This arbitrariness, however, may be eliminated. To satisfy conservation of mass the integral of $f_1'(\chi)$ in 0 to $2\alpha_m$ must be zero, therefore

$$A_1 = -\frac{2I_1}{7\alpha_m^2} \quad (4.44)$$

and if ϵ is defined such that it is proportional to the leading order wave height then the inner product of η_0 with η_1 should be zero. This gives a value for A_2 of

$$A_2 = -2\frac{\omega_1}{\alpha_m^2} + \frac{33I_4}{7I_1\alpha_m} \quad (4.45)$$

Therefore substitution of (4.43)-(4.45) into (4.36) and (4.37) gives a complete description for the first order solution.

In Figure 4.1 a bifurcation diagram for the frequency is shown. ω_1 is positive definite and it appears that ω_2 is as well so the bifurcation is subcritical for all the modes; the natural frequency of the cnoidal standing waves increases with increasing amplitude. A typical time series for the wave height at the left tank wall is given in Figure 4.2.

In Figure 4.3, the evolution of the mode=1 cnoidal standing wave is shown. The result is plotted as a function of space with each successive frame $\frac{1}{20}^{th}$ of a temporal period. This wave is very similar to that found by Vanden-broeck and Schwartz [18], using a numerical technique, and shown in their Figure 3. Figures 4.4 and 4.5 show the evolution of a 2-mode and 3-mode respectively. The "travelling character" of these waves is to be contrasted with the "standing character" of the elliptic standing waves. In Figure 4.6 the evolution of a 1 mode elliptic standing wave is plotted. Here the wave appears to move vertically and otherwise remain coherent. Figure 4.7 shows the evolution of a 3-mode elliptic standing wave.

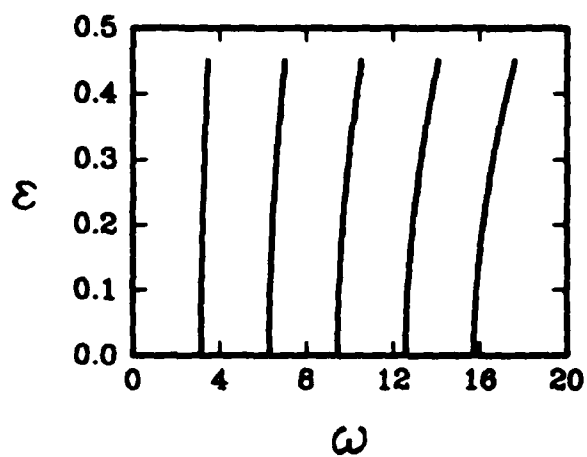


Figure 4.1 Bifurcation diagram for the natural frequency (the first five modes) of standing cnoidal waves.

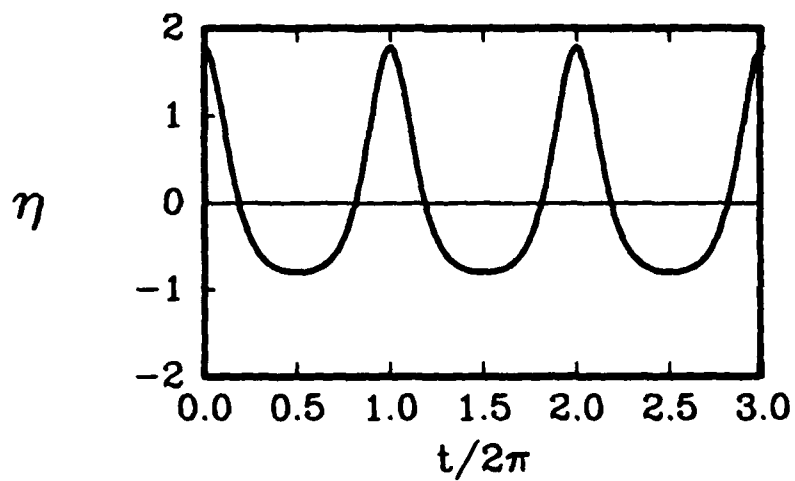
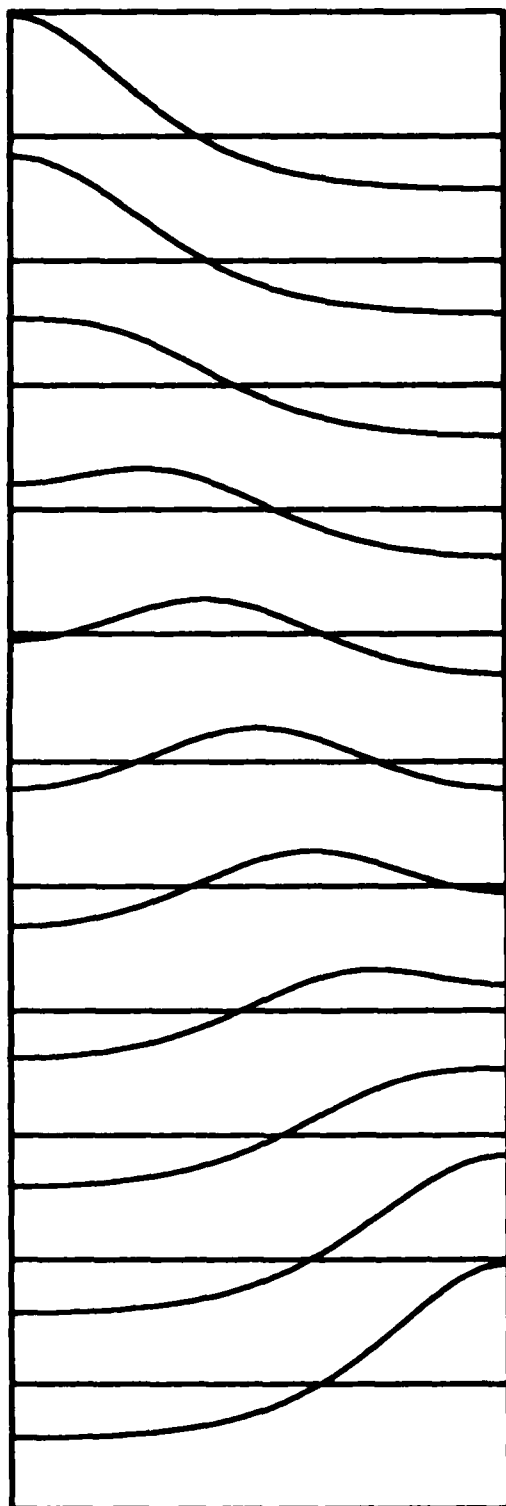


Figure 4.2 Time series for the wave height at the left tank wall for a cnoidal standing wave.

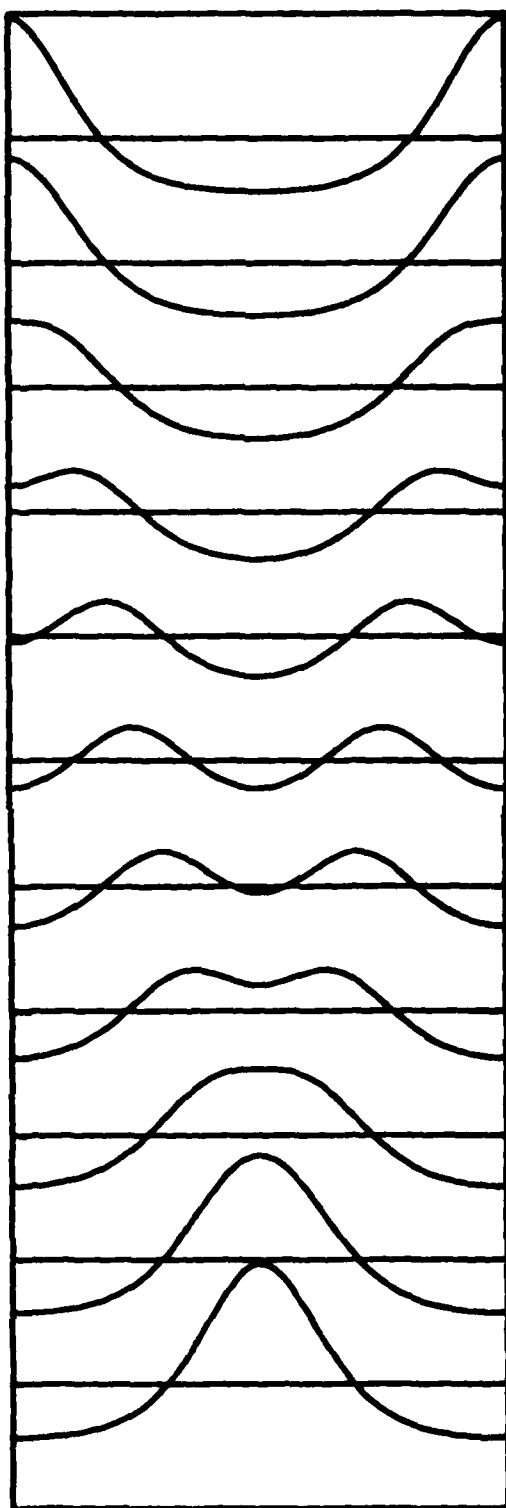


$$t = 0$$

Figure 4.3 Temporal evolution of the x-distribution of the wave height for a 1-mode cnoidal standing wave.

$$t = \frac{1}{2} \pi$$

$$t = \pi$$

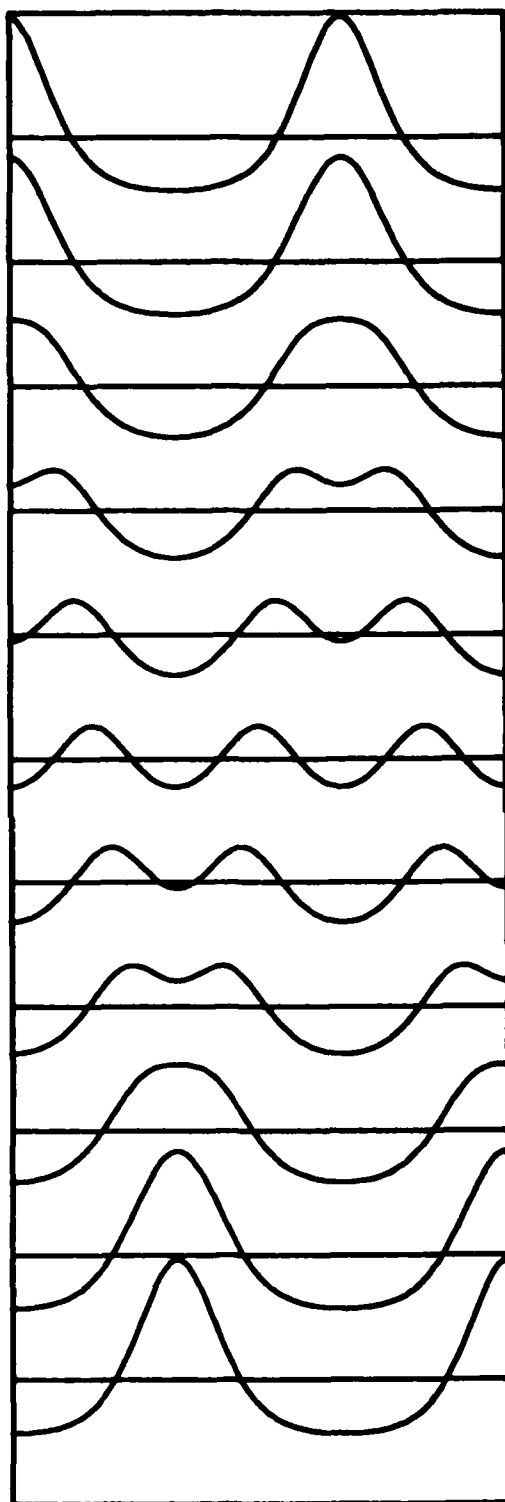


$t = 0$

Figure 4.4 Temporal evolution of the x-distribution of the wave height for a 2-mode cnoidal standing wave.

$t = \frac{1}{2}\pi$

$t = \pi$

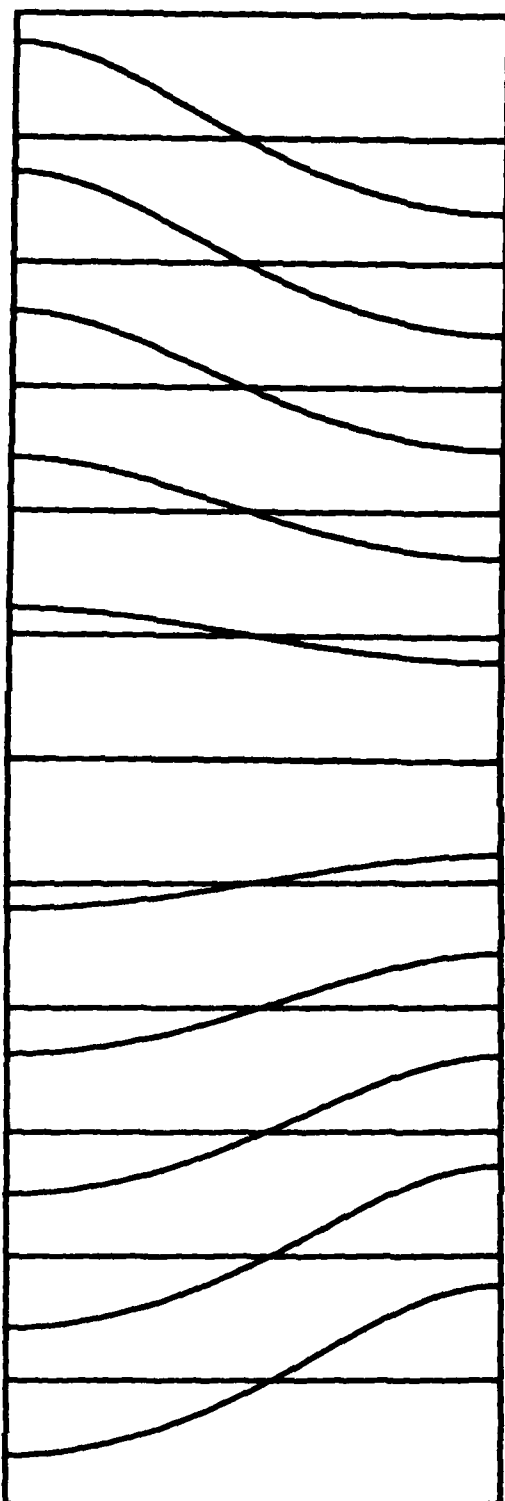


$t = 0$

Figure 4.5 Temporal evolution of the x-distribution of the wave height for a 3-mode cnoidal standing wave.

$t = \frac{1}{2} \pi$

$t = \pi$

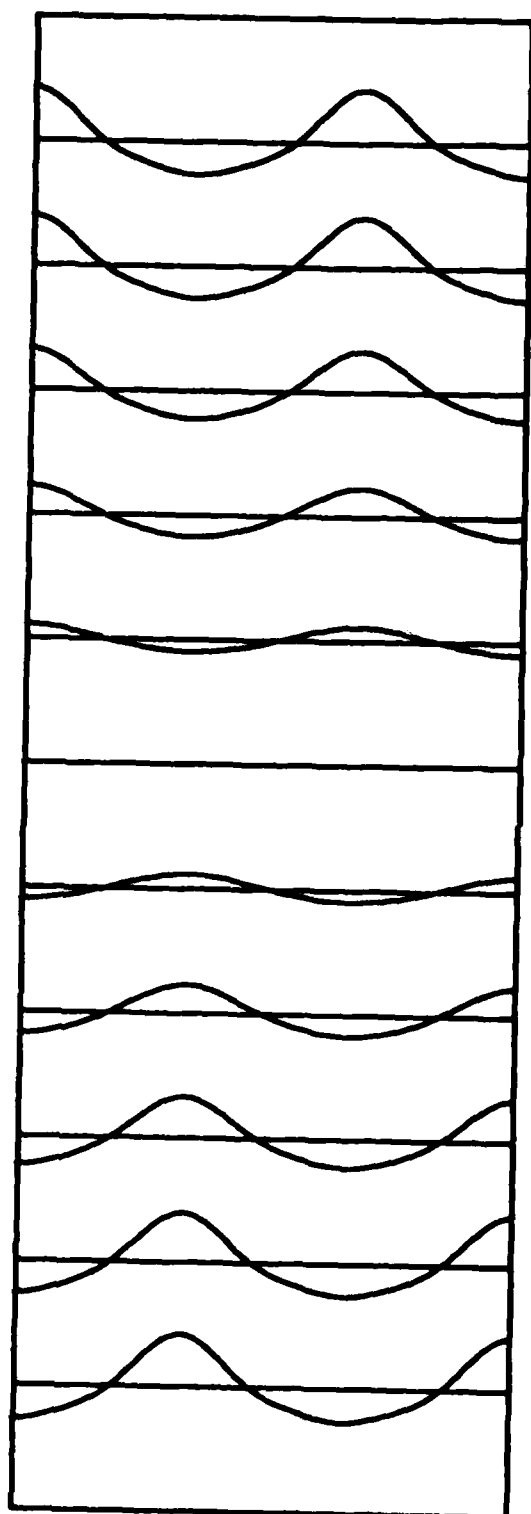


$$t = 0$$

Figure 4.6 Temporal evolution of the x-distribution of the wave height for a 1-mode *elliptic* standing wave.

$$t = \frac{1}{2}\pi$$

$$t = \pi$$



$$t = 0$$

Figure 4.7 Temporal evolution of the x-distribution of the wave height for a 3-mode *elliptic* standing wave.

$$t = \frac{1}{2}\pi$$

$$t = \pi$$

The distribution of the 2-mode at $t = \pi$ at the bottom of Figure 4.4 raises an interesting question about the enclosed angle of the crest of a large amplitude cnoidal standing wave. It is well known that the Stokes wave has a limiting angle of 120° . Schwartz and Whitney [14] have shown that the elliptic standing wave probably has a limiting angle of 90° . The cnoidal standing wave appears to have a limiting angle less than 90° , probably much less than 90° , and possibly a limiting configuration that is a cusp.

The cnoidal standing wave is the periodic surface wave occurring when the fluid is shallow and $\epsilon = O(\delta^2)$. When $\epsilon \gg \delta^2$ it was shown that no periodic solutions exist to the innate problem although a hydraulic jump is formed in response to a forcing function. There is obviously a vague region remaining between $\epsilon = O(\delta^2)$ and $\epsilon \gg \delta^2$. The transition from a cnoidal standing wave to a hydraulic jump is an interesting but still unclear theoretical problem. In the next section experimental observations of cnoidal standing waves as well as another class of waves witnessed between $\epsilon = O(\delta^2)$ and $\epsilon \gg \delta^2$ will be elaborated.

5. Experimental Study of the Transition Region

The transition region is defined to be the region in the amplitude, ϵ , with fixed and small δ , after the breakdown of the elliptic standing waves and before the formation of the hydraulic jump. It was shown in the previous section that the eigenfunction for the nonlinear problem in this region is the cnoidal standing wave. The first step is to see if such waves are observed in the experiment. It will be shown that this, in fact, is the case. The parameters are chosen such that an isolated 1-mode cnoidal standing wave occurs. The depth parameter is $\delta \sim 0.2$, and the forcing frequency is $f = 1.0$ which is just above the first linear natural frequency $f_1 \sim 0.97$. The photos in Figures 5.1, 5.2, and 5.3 are of this wave at three different times. The wave has the distinct undulating motion associated with the cnoidal standing wave and not observed in the elliptic standing wave which has (almost) a node at the center of the tank. Comparing Figures 5.1-5.3 with Figure 4.3 it is seen that 5.2 resembles the evolution in 4.3 at $t = (9 \text{ or } 10) \frac{\pi}{10}$, 5.2 at $t = (6 \text{ or } 7) \frac{\pi}{10}$ and 5.3 at $t = \frac{\pi}{2}$. Figure 5.4a is the time series for the wave height at the left tank wall for the wave in Figure 5.1-5.3 and Figure 5.4b is the Log of the Fourier transform of this time series. The time series closely resembles that predicted by the cnoidal wave theory in Figure 4.2.

The eigenfunction analysis of the previous sections has suggested that the eigenfunctions when $\epsilon \ll \delta^2$ are the elliptic standing waves, and when $\epsilon = O(\delta^2)$ the eigenfunctions are the cnoidal standing waves, and when $\epsilon \gg \delta^2$ it was suggested that there are no periodic characteristic solutions. It is possible that there is another class of eigenfunctions between $\epsilon = O(\delta^2)$ and $\epsilon \gg \delta^2$ but this is unlikely. These remarks serve as an introduction to the experimental observations which follow.



Figure 5.1 A 1-mode cnoidal standing wave at peak amplitude when $\delta \sim 0.2$, $f_1 = .97$, and $f = 1.0$.

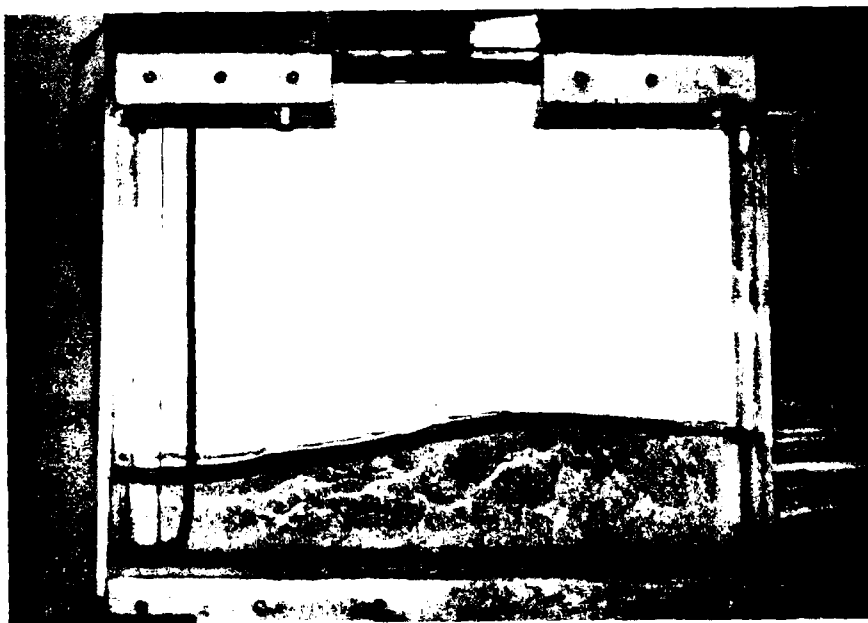


Figure 5.2 A 1-mode cnoidal standing wave at a different time with $\delta \sim 0.2$, $f_1 = .97$, and $f = 1.0$.

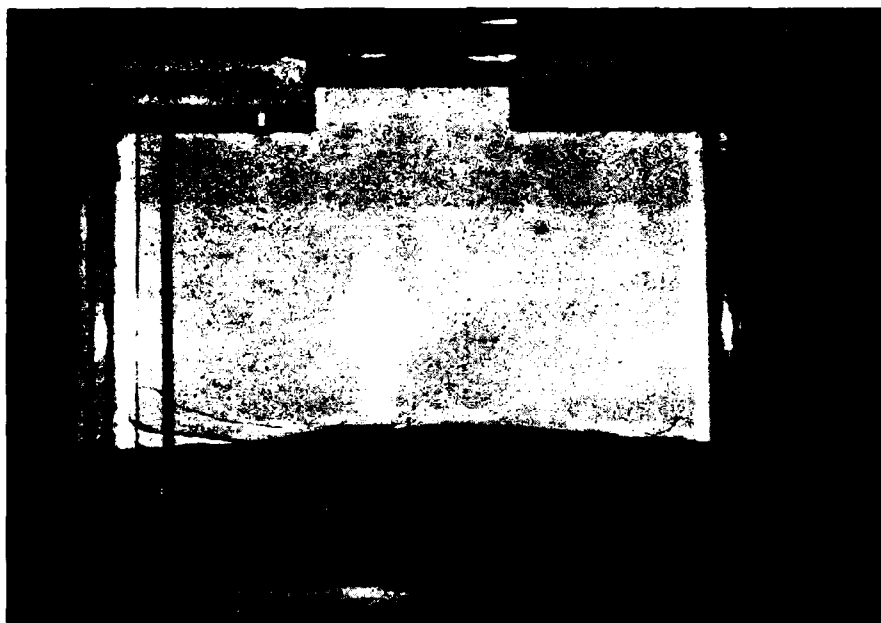


Figure 5.3 A additional 1-mode cnoidal standing wave at a different time with $\delta \sim 0.2$, $f_1 = .97$, and $f = 1.0$.

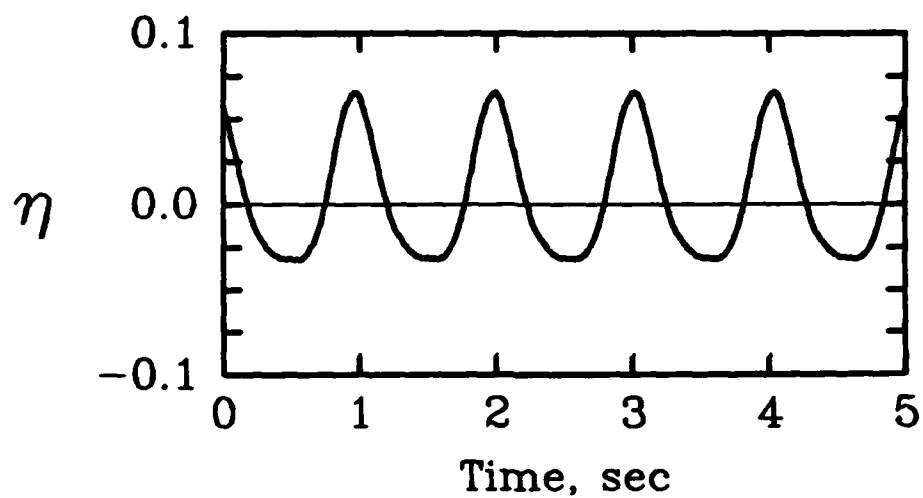


Figure 5.4a The time series for the wave height at the left tank wall corresponding to Figures 5.1-5.3. The parameters are $\delta \sim 0.2$, $f_1 = .97$, and $f = 1.0$.

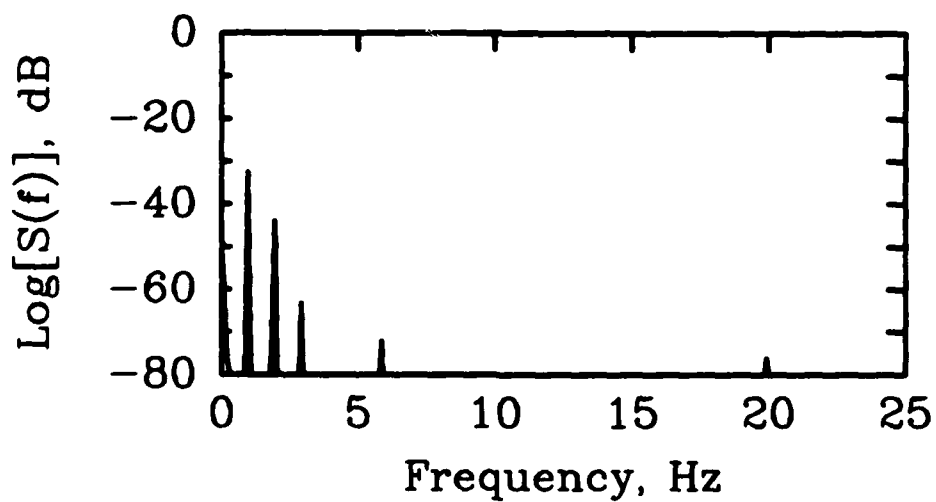


Figure 5.4b The Log magnitude of the Fourier transform of the time series in Figure 5.4a.

The complex waves observed, as the amplitude increases and the "clean" 1-mode cnoidal standing wave changes into a wave field with greater spatial complexity, are probably due to the selecting process of the forcing function which is present. So rather than a new class of eigenfunctions these waves are probably compound cnoidal waves and in fact the observations lend credence to this judgement. There are two distinct compound waves which occur so often (for a large but compact range of parameters) that they may be given titles. They are the compound 1-3 wave and the compound wiggle wave. The compound 1-3 wave appears at shallow depths but not too shallow ($\delta > 0.15$) and looks like a cnoidal 1-mode joined with a cnoidal 3-mode. Figures 5.5 and 5.6 are photos of the compound 1-3 wave at two different times showing (almost) the symmetry. The forcing is at the first natural frequency but the presence of the third mode is quite obvious. This wave has a rather interesting time series as well and it is shown in Figure 5.7a with its Fourier transform in Figure 5.7b. The time series is periodic with an obvious presence of higher harmonics.

The compound wiggle wave occurs at shallower depths at sufficient amplitude. Figures 5.8-5.11 show an example of this wiggle wave at four different times. The depth is $\delta = .084$ and the forcing frequency equals the linear natural frequency. The wave is periodic, repeatable, and deterministic but has many spatial harmonics (most notably a 5-mode in Figure 5.10) and the harmonics travel at different speeds from the fundamental. A time series for this wiggle wave is given in Figure 5.12a, with its Fourier transform in Figure 5.12b, where the "wiggles" are quite apparent. The Fourier transform also suggests that these harmonics are integral multiples of the fundamental. It is interesting to note that the compound wiggle wave is always a prelude to the hydraulic jump. If a compound wiggle wave is formed and the amplitude, of the forcing function, is increased further a threshold is reached where the wave changes (bifurcates?) into a travelling hydraulic jump.

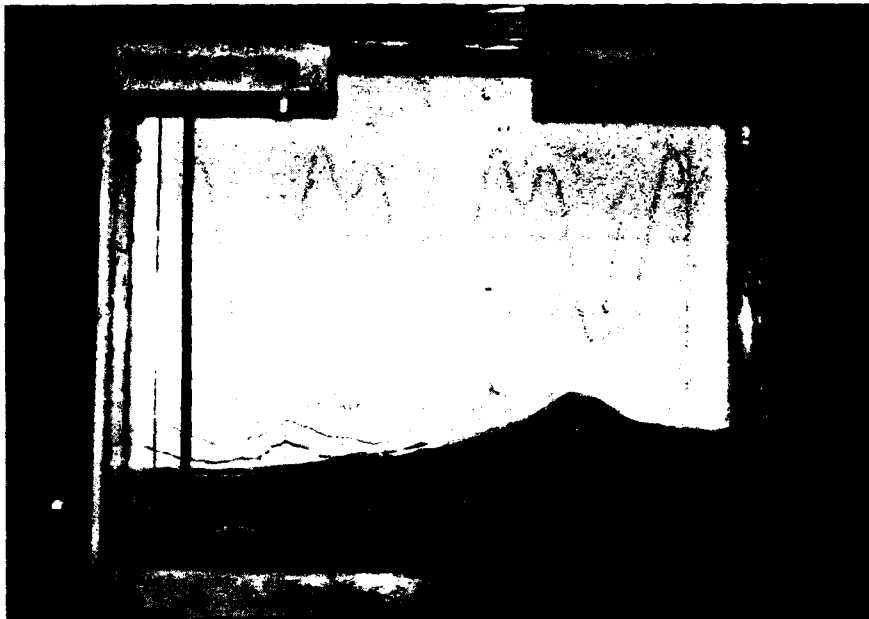


Figure 5.5 A photo of the compound 1-3 standing wave. The parameters are $\delta \sim 0.17$, $f_1 = .91$, and $f = .95$. Although the forcing frequency is near the first mode, a 3-mode in space is present.



Figure 5.6 Same wave and parameters as Figure 5.5 but at a different time.

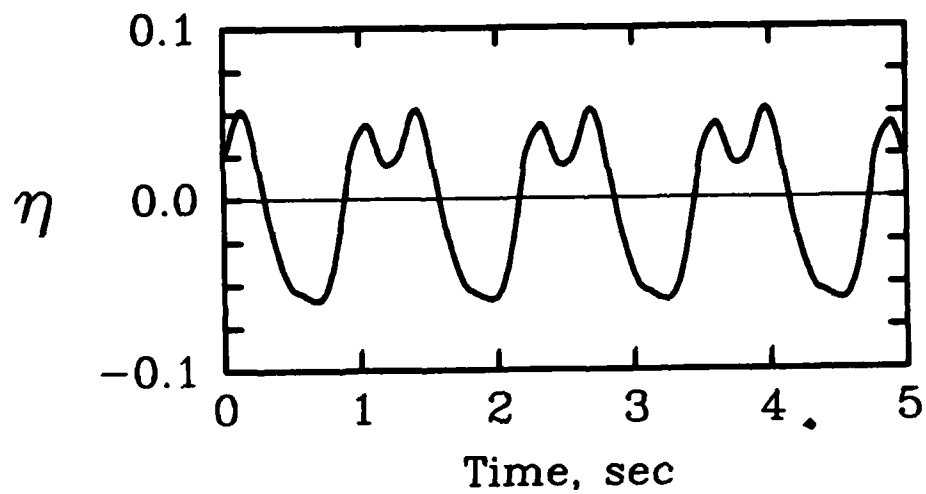


Figure 5.7a Time series at the left tank wall for the compound 1-3 standing wave. The parameters are $\delta \sim 0.17$, $f_1 = .91$, and $f = .95$.

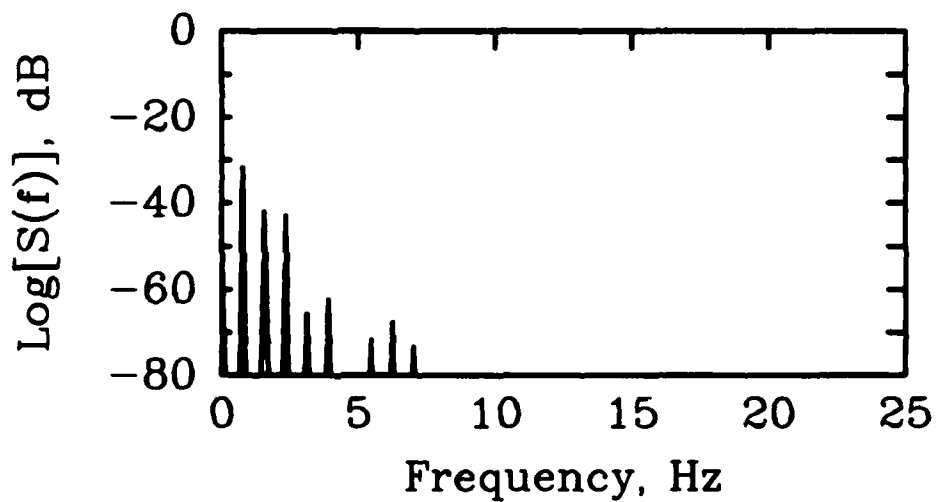


Figure 5.7b The Log magnitude of the Fourier transform of the time series in Figure 5.7a.

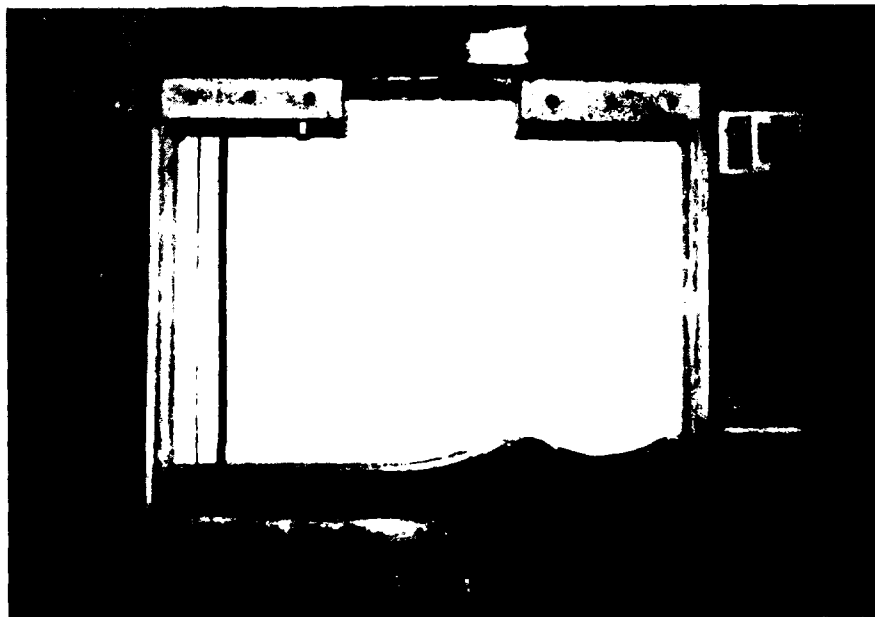


Figure 5.8 A compound wobble wave in shallow water. The parameters are $\delta = .084$, $f_1 = .6655$, and $f = .67$.

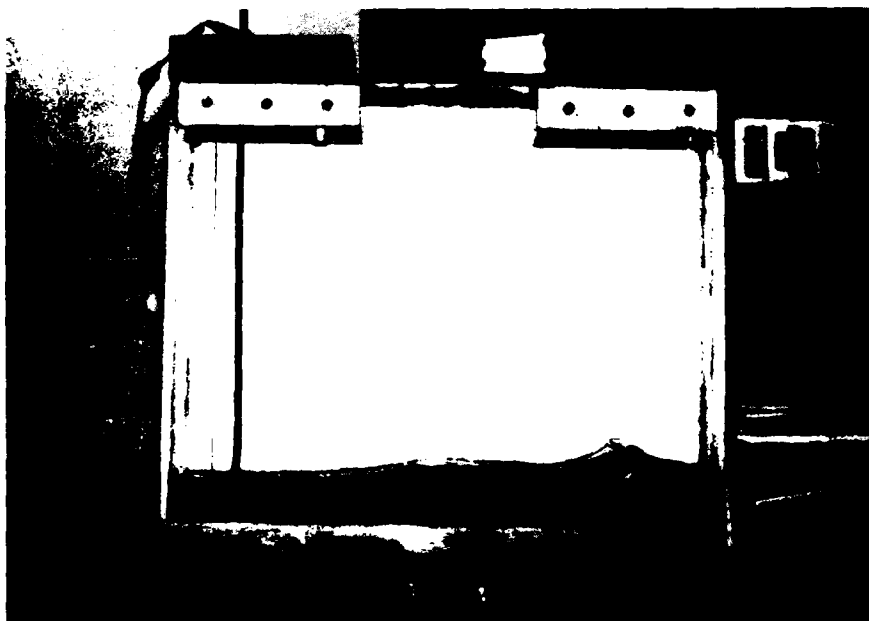


Figure 5.9 A compound wobble wave with the same parameters as Figure 5.8 at a different time showing how the wave crests travel independently.

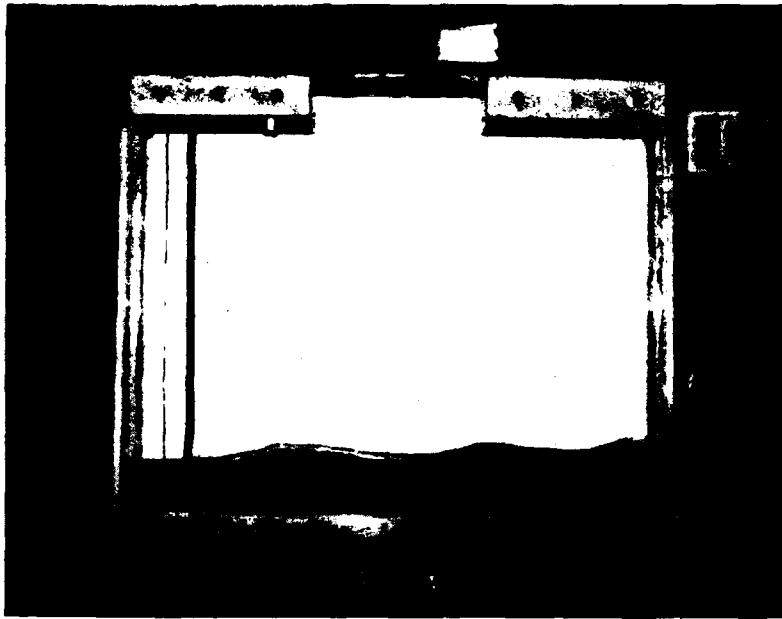


Figure 5.10 A compound wobble wave with the same parameters as Figure 5.8 at a different time. Here the wave is characteristic of a 5-mode standing wave suggesting its presence.

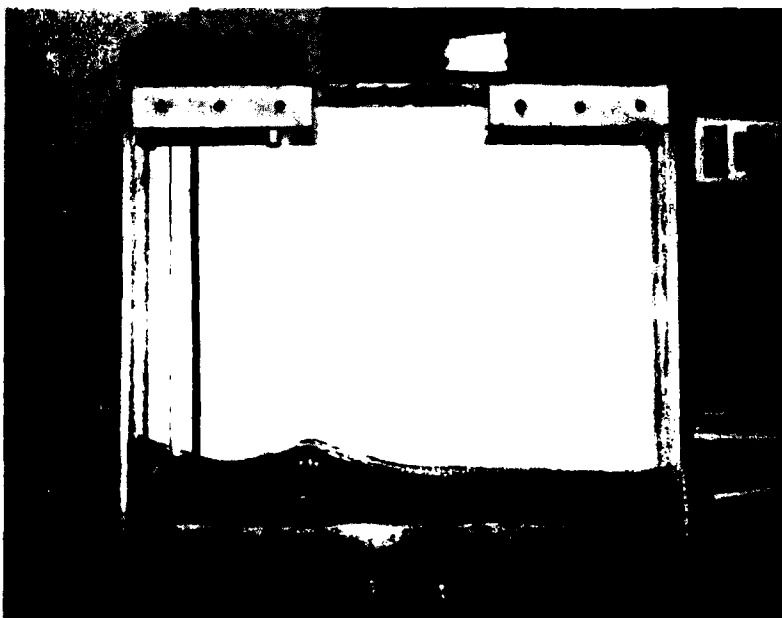


Figure 5.11 A compound wobble wave with the same parameters as Figure 5.8 at $\frac{1}{2}$ a period later than Figure 5.8.

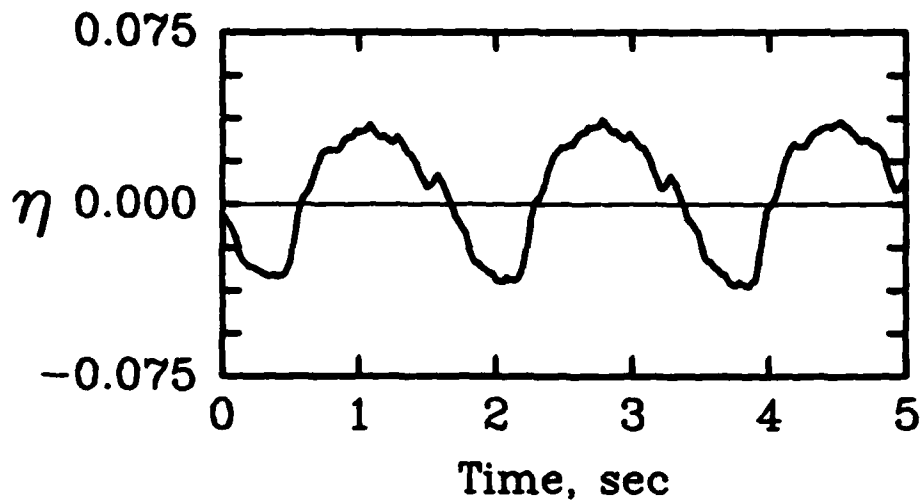


Figure 5.12a Time series for the wave height at the left tank wall for the compound wiggly wave. The parameters are $\delta = .098$, $f_1 = .716$, and $f = .67$. The wave form is living up to its name but remains periodic.

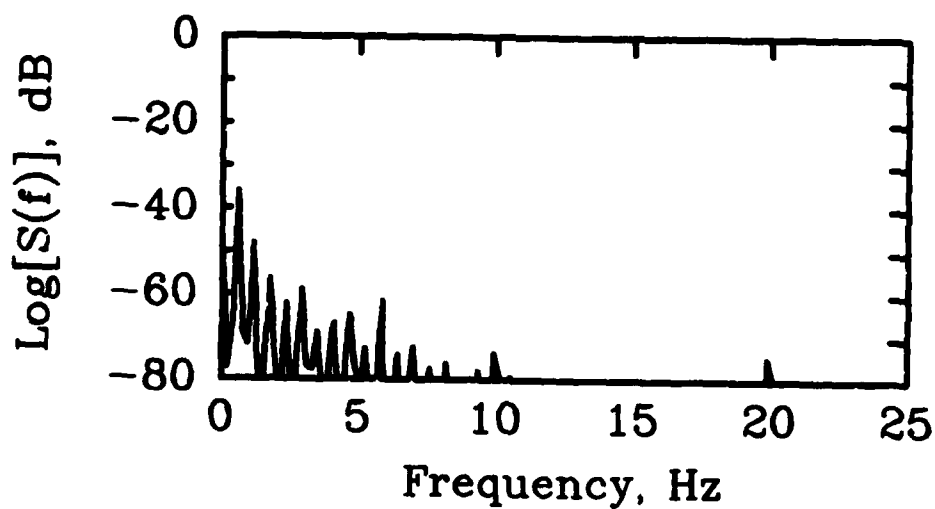


Figure 5.12b The Log magnitude of the Fourier transform of the time series in Figure 5.12a.

Figure 5.13 shows an example of another variety of compound wiggle wave in deeper water. Figures 5.14-5.17 are four other interesting time series which were observed and are worthy of mention. Figures 5.14, 5.15 are of two different compound wiggle waves showing the increase in harmonic complexity as the amplitude increases and Figure 5.16, 5.17 are time series of the wave height for ordinary 1-mode cnoidal standing waves as they become more nonlinear. These observations lead to a cascade hypothesis.

The following scenario may be constructed based upon the observations recorded in the figures in this section. When $\epsilon = O(\delta^2)$ the solution observed is that of a cnoidal standing wave which closely resembles the eigenfunction. As the amplitude is increased such that it is slightly greater than $O(\delta^2)$ the third mode natural frequency becomes closer to three times the first mode. This brings in the 3-mode cnoidal standing wave forming the compound 1-3 standing wave observed in Figures 5.5-5.7. Now as the amplitude is increased further relative to δ^2 a point is reached such that the 5-mode cnoidal standing wave is excited. This produces the compound wiggle wave observed in Figures 5.7-5.14. As the amplitude is further increased relative to δ^2 the cascade of higher harmonics continues until the dispersion is so small that it no longer can check the flood of harmonics and a travelling hydraulic jump is formed.

In other words as ϵ increases to $\epsilon \gg \delta^2$ with δ^2 sufficiently small, the higher natural frequencies become closer and closer to being integral multiples of the fundamental, and apparently this occurs in order of increasing mode number causing the cascade process described above.

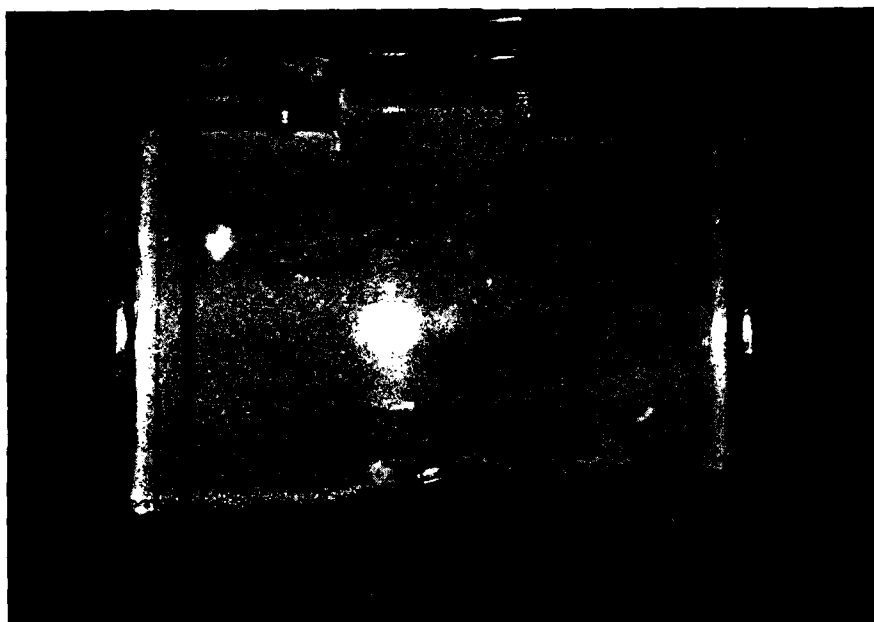


Figure 5.13 A photo of a compound wiggle wave when the water is deeper. The parameters are $\delta = 0.12$, $f_1 = .76$, and $f = .7$. In spite of a 50% increase in depth the character of this wave remains the same.

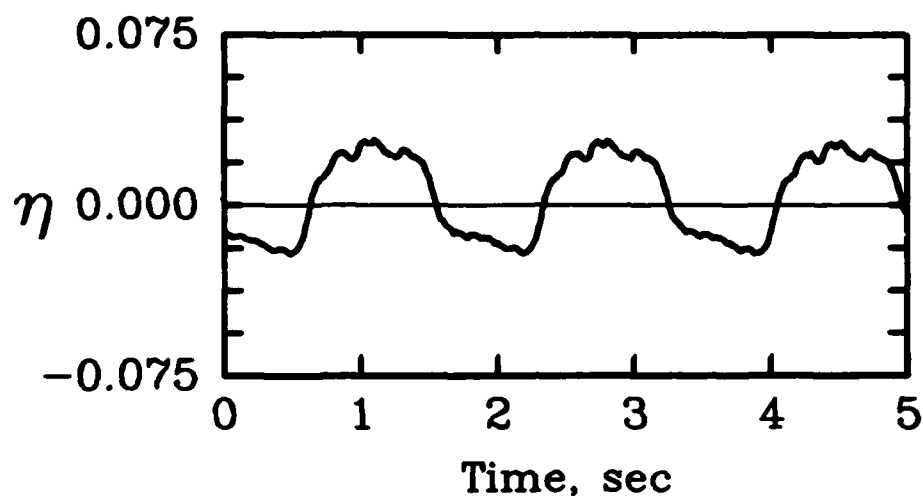


Figure 5.14 A variation of the time series for the compound wiggly wave. The parameters are $\delta = .08$, $f_1 = .6655$, and $f = .67$. This time series corresponds to the photos in Figures 5.8-5.11.

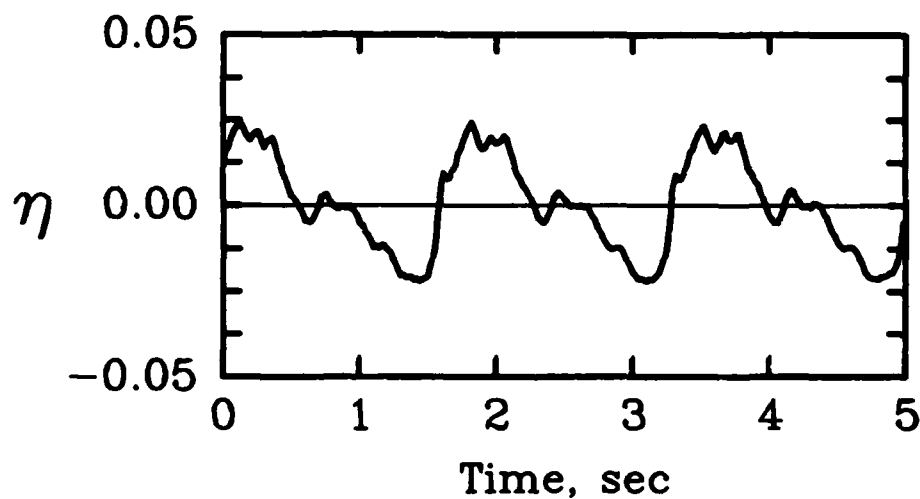


Figure 5.15 The time series for a further variation of the compound wiggly wave when $\delta = 0.07$, $f_1 = .61$, and $f = .6$. Although the wave remains periodic there is a rich set of harmonics present.

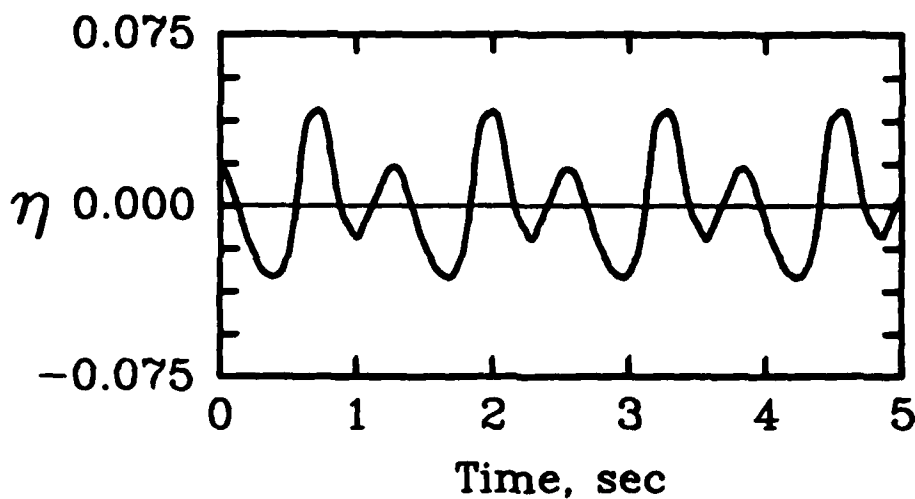


Figure 5.16 A time series for a 1-mode cnoidal standing wave of large amplitude. Although (spatially) in appearance this wave resembles a 1-mode cnoidal standing wave it has reached sufficient amplitude to require higher order terms. The parameters are $\delta = .14$, $f_1 = .84$, and $f = .84$.

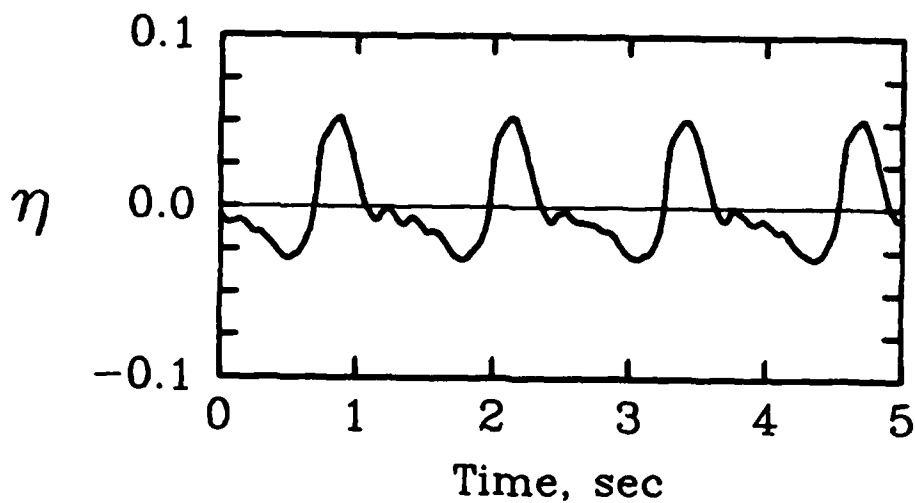


Figure 5.17 A time series for another variation of the nonlinear 1-mode cnoidal standing wave. The parameters are $\delta = .112$, $f_1 = .762$, and $f = .8$.

Appendix I

A coordinate system $S(X, Y, Z)$ is fixed in Newtonian space and a second coordinate system $S'(x, y, z)$ is attached to the center of the undisturbed water level of a three dimensional partially filled cuboidal container. From the theory of dynamics it is well known that when the coordinate system S' is accelerating relative to the fixed system S , the relationship between the absolute and relative acceleration is

$$\vec{A} = \vec{a} + 2\vec{\Omega} \times \vec{u} + \dot{\vec{\Omega}} \times \vec{r} + \vec{\Omega} \times \vec{\Omega} \times \vec{r} + \dot{\vec{\Omega}} \times \vec{d} + \vec{\Omega} \times \vec{\Omega} \times \vec{d} \quad (I.1)$$

where $\vec{\Omega}$ is the angular velocity of the vessel and \vec{d} is the fixed distance between the origins of S and S' . This expression is substituted into the Euler equations of motion for an inviscid fluid to obtain the governing equations for the fluid in the vessel relative to S' ,

$$\begin{aligned} \frac{D\vec{u}}{Dt} + 2\vec{\Omega} \times \vec{u} + \dot{\vec{\Omega}} \times (\vec{r} + \vec{d}) + \vec{\Omega} \times \vec{\Omega} \times (\vec{r} + \vec{d}) = \\ -\frac{1}{\rho} \nabla p + g \nabla h \end{aligned} \quad (I.2)$$

where h is the elevation above some datum. Because of the presence of $\vec{\Omega}$ the fluid motion is not irrotational. However if it is assumed that the vorticity is strictly due to the rigid body motion of the vessel the velocity field can be decomposed into

$$\vec{u} = \nabla \phi - \vec{\Omega} \times \vec{r} \quad (I.3)$$

and the motion relative to S' is assumed to be irrotational. The governing equation is then the Laplace equation in the interior of the fluid and substitution of (I.3) into (I.2) results in a modified Bernoulli equation for the pressure,

$$\begin{aligned} \frac{\partial \phi}{\partial t} + \frac{1}{2} \nabla \phi \cdot \nabla \phi - \vec{\Omega} \times \vec{r} \cdot \nabla \phi + \frac{1}{2} (\vec{\Omega} \times \vec{r}) \cdot (\vec{\Omega} \times \vec{r}) \\ + \frac{p}{\rho} + gh + (\dot{\vec{\Omega}} \times \vec{d} + \vec{\Omega} \times \vec{\Omega} \times \vec{d}) \cdot \vec{r} = f(t) \end{aligned} \quad (I.4)$$

However reducing the problem to two spatial dimensions, as in Figure 1.1, where the vessel rotates about some fixed point P, results in the set of equations given in Section 1.

Appendix II

In this appendix the coefficients for the second order velocity potential and wave height for the elliptic standing wave are given.

$$A_{21} = \frac{1}{256\sigma_0} \left[\frac{3\alpha_m^6}{\sigma_0^8\delta^2} + \frac{9\alpha_m^4}{\sigma_0^4} - 5\alpha_m^2\delta^2 - 13\sigma_0^4\delta^4 + \frac{6\sigma_0^8\delta^6}{\alpha_m^2} \right] \quad (II.1)$$

$$A_{22} = \frac{1}{256\sigma_0} \left[\frac{9\alpha_m^6}{\sigma_0^8\delta^2} + \frac{62\alpha_m^4}{\sigma_0^4} - 31\alpha_m^2\delta^2 \right] \quad (II.2)$$

$$A_{23} = \frac{1}{256\sigma_0} \left[-\frac{9\alpha_m^8}{\sigma_0^{12}\delta^4} - \frac{5\alpha_m^6}{\sigma_0^8\delta^2} + \frac{52\alpha_m^4}{\sigma_0^4} - 39\alpha_m^2\delta^2 \right] \quad (II.3)$$

$$B_{21} = \frac{1}{64} \left[\frac{3\alpha_m^6}{\sigma_0^8\delta^2} + \frac{6\alpha_m^4}{\sigma_0^4} - 5\alpha_m^2\delta^2 + 2\sigma_0^4\delta^4 \right] \quad (II.4)$$

$$B_{22} = \frac{3}{256} \left[\frac{9\alpha_m^6}{\sigma_0^8\delta^2} + \frac{27\alpha_m^4}{\sigma_0^4} - 15\alpha_m^2\delta^2 + \frac{2\sigma_0^8\delta^6}{\alpha_m^2} \right] \quad (II.5)$$

$$B_{23} = \frac{1}{256} \left[\frac{3\alpha_m^6}{\sigma_0^8\delta^2} + \frac{18\alpha_m^4}{\sigma_0^4} - 5\alpha_m^2\delta^2 \right] \quad (II.6)$$

$$B_{24} = \frac{3}{256} \left[-\frac{9\alpha_m^8}{\sigma_0^{12}\delta^4} + \frac{3\alpha_m^6}{\sigma_0^8\delta^2} - \frac{3\alpha_m^4}{\sigma_0^4} + am^2\delta^2 \right] \quad (II.7)$$

Appendix III

In this appendix a theorem for the solvability of the inhomogeneous wave equation is given. A variation of this solvability condition, when $m=1$ and the boundary conditions are dirichlet, was first derived by Keller and Ting[8] and used by them to prove non-existence of periodic solutions for a class of nonlinear wave equations. It is used here to prove existence, albeit formal existence, for the nonlinear wave equation governing standing waves.

Theorem: *Given the inhomogeneous wave equation,*

$$\omega_0^2 \frac{\partial^2 \Upsilon}{\partial t^2} - \frac{\partial^2 \Upsilon}{\partial x^2} = F(x, t), \quad 0 \leq x \leq 1, \quad -\infty < t < \infty \quad (III.1)$$

$$\frac{\partial \Upsilon}{\partial x}(0, t) = \frac{\partial \Upsilon}{\partial x}(1, t) = 0 \quad (III.2)$$

where $\omega_0 = \alpha_m = m\pi$, m is any integer greater than zero, Υ_x , Υ_t , and F are periodic in time with period 2π , $F(x, t)$ is an even function of x , and in addition satisfies

$$F(x + 1, t + \pi) = F(x, t), \quad (III.3)$$

then there is a solution to the inhomogeneous problem if and only if

$$\int_0^{2\alpha_m} F\left[\frac{\xi - \chi}{2\alpha_m}, \frac{\xi + \chi}{2}\right] d\xi = 0 \quad (III.4)$$

Proof: Every solution of the homogeneous problem

$$\omega_0^2 \frac{\partial^2 \Psi}{\partial t^2} - \frac{\partial^2 \Psi}{\partial x^2} = 0, \quad 0 \leq x \leq 1, \quad -\infty < t < \infty \quad (III.5)$$

$$\frac{\partial \Psi}{\partial x}(0, t) = \frac{\partial \Psi}{\partial x}(1, t) = 0 \quad (III.6)$$

which is 2π periodic in time may be expressed as

$$\Psi(x, t) = f(t + \alpha_m x) + f(t - \alpha_m x) \quad (III.7)$$

Multiply (III.1) by $\Psi(x, t)$ and integrate from 0 to 1 in x and 0 to 2π in t . Integration by parts and the end and periodicity conditions result in the left hand side becoming zero, then

$$\int_0^{2\pi} \int_0^1 \Psi(x, t) F(x, t) dx dt = 0 \quad (III.8)$$

For the higher modes the integrand may be expanded in x taking advantage of the even extension of $F(x, t)$ to all x ,

$$\frac{1}{m} \int_0^{2\pi} \int_{-\frac{m}{2}}^{\frac{m}{2}} \Psi(x, t) F(x, t) dx dt = 0 \quad (III.9a)$$

when m is even and

$$\frac{1}{m} \int_0^{2\pi} \int_{-\frac{(m-1)}{2}}^{\frac{(m+1)}{2}} \Psi(x, t) F(x, t) dx dt = 0 \quad (III.9b)$$

when m is odd.

Now a change of variable is made to

$$\xi = t + \alpha_m x \quad (III.10a)$$

$$\chi = t - \alpha_m x \quad (III.10b)$$

The region of integration in the ξ, χ plane for the first and second modes is shown in Figure III.1. The higher modes have regions of a similar nature. With the change of variables (III.10), and use of (III.3), and the fact that the integrand is similar in any period parallelogram in Figure III.1, the integral (III.9) becomes

$$\int_0^{2\alpha_m} \int_0^{2\alpha_m} \left[f(\xi) + f(\chi) \right] F \left[\frac{\xi - \chi}{2\alpha_m}, \frac{\xi + \chi}{2} \right] d\xi d\chi = 0 \quad (III.11)$$

which may be written as the sum of two integrals $f(\xi)F$ and $f(\chi)F$. In the first of these the variables of integration are interchanged. Since F is even in x the sum becomes

$$2 \int_0^{2\alpha_m} f(\chi) \int_0^{2\alpha_m} F \left[\frac{\xi - \chi}{2\alpha_m}, \frac{\xi + \chi}{2} \right] d\xi d\chi = 0 \quad (III.13)$$

As a consequence of the arbitrariness of $f(\chi)$, this implies (III.4) and proves the theorem.

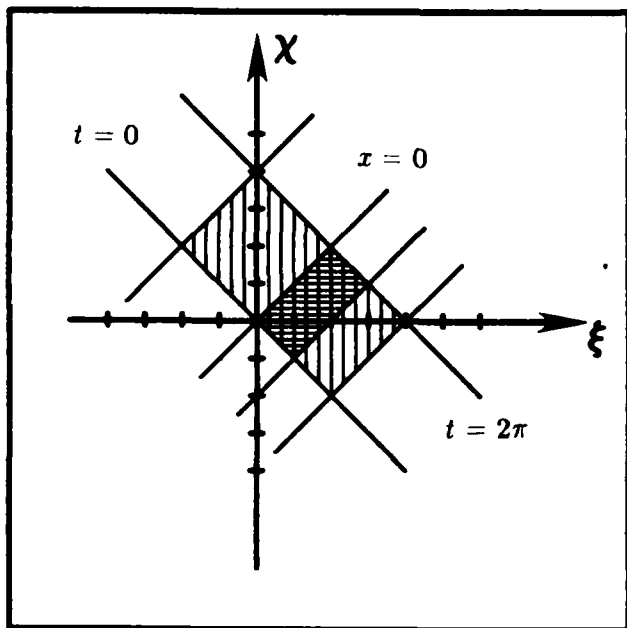


Figure III.1 The range of integration in the transformed domain for mode 1 and 2. The region with horizontal stripes is for $m=1$ and the vertical striped region is for $m=2$.

Appendix IV

In this appendix the details of the Jacobian Elliptic functions necessary for the construction of the cnoidal standing wave solutions are given. They are taken from the *Handbook of Elliptic Integrals* [1].

The complete elliptic integral of the first kind is

$$K\left(\frac{\pi}{2}; \kappa\right) = \int_0^{\frac{\pi}{2}} \frac{d\zeta}{\sqrt{1 - \kappa^2 \sin^2 \zeta}} \quad (IV.1)$$

where in the standing wave problem $K(\frac{\pi}{2}; \kappa) = \pi$. The incomplete elliptic integral of the second kind is

$$E(x; \kappa) = \int_0^x \left[1 - \kappa^2 + \kappa^2 \operatorname{cn}^2(\zeta; \kappa) \right] d\zeta \quad (IV.2)$$

which when $K(\frac{\pi}{2}; \kappa) = \pi$ has the completed form

$$E(\pi; \kappa) = \int_0^{\frac{\pi}{2}} \sqrt{1 - \kappa^2 \sin^2 \zeta} d\zeta \quad (IV.3)$$

The Jacobi Zeta function is

$$Z(x; \kappa) = E(x; \kappa) - \frac{E(\pi; \kappa)}{K(\frac{\pi}{2}; \kappa)} x \quad (IV.4)$$

which has the complete Fourier series

$$Z(x; \kappa) = \frac{2\pi}{K(\frac{\pi}{2}; \kappa)} \sum_{n=1}^{\infty} \frac{q^n}{1 - q^{2n}} \sin \left[\frac{n\pi x}{K(\frac{\pi}{2}; \kappa)} \right] \quad (IV.5)$$

where $q = \exp(-\pi K(\frac{\pi}{2}; \kappa')/K(\frac{\pi}{2}; \kappa))$ and $\kappa' = \sqrt{1 - \kappa^2}$ and the cnoidal function has the Fourier series

$$\operatorname{cn}^2(x; \kappa) = \sum_{n=0}^{\infty} A_n \cos \left[\frac{n\pi x}{K(\frac{\pi}{2}; \kappa)} \right] \quad (IV.6)$$

where

$$A_0 = \frac{1}{\kappa^2} \left[\frac{E(\pi; \kappa)}{K(\frac{\pi}{2}; \kappa)} + \kappa^2 - 1 \right] \quad (IV.7a)$$

and

$$A_n = \frac{2\pi^2}{\kappa^2 K^2(\frac{\pi}{2}; \kappa)} \frac{nq^n}{1 - q^{2n}}, \quad \text{for } n > 0 \quad (IV.7b)$$

The constants d_1, d_2 used in the expression for ω_2 in Section 4 are

$$d_1 = 12\kappa^2 \frac{A^2}{B} - 4B(1 - \kappa^2) + 8A(2\kappa^2 - 1) \quad (IV.8a)$$

$$d_2 = -6\kappa^2 \frac{A}{B} - 2(2\kappa^2 - 1) \quad (IV.8b)$$

where A and B are defined in Section 4. The integrals used in the first order solution as well as ω_2 are now given where $C_p = \int_0^{2\alpha_m} \text{cn}^p(\zeta; \kappa) d\zeta$ and $K(\frac{\pi}{2}; \kappa) = \pi$

$$C_2 = \frac{2\alpha_m}{\kappa^2} \left[\kappa^2 - 1 + \frac{E(\pi; \kappa)}{\pi} \right] \quad (IV.9a)$$

$$C_4 = \frac{2\alpha_m}{3\kappa^4} \left[(2 - 3\kappa^2)(1 - \kappa^2) + 2(2\kappa^2 - 1) \frac{E(\pi; \kappa)}{\pi} \right] \quad (IV.9b)$$

$$C_6 = \frac{4(2\kappa^2 - 1)C_4 + 3(1 - \kappa^2)C_2}{5\kappa^2} \quad (IV.9c)$$

$$C_8 = \frac{6(2\kappa^2 - 1)C_6 + 5(1 - \kappa^2)C_4}{7\kappa^2} \quad (IV.9d)$$

and

$$\begin{aligned} I_2 &= \int_0^{2\alpha_m} h'(\zeta) h'(\zeta) d\zeta \\ &= \frac{8\alpha_m B^2}{15\kappa^4} \left[(\kappa^2 - 2)(1 - \kappa^2) + 2(\kappa^4 - \kappa^2 + 1) \frac{E(\pi; \kappa)}{\pi} \right] \end{aligned} \quad (IV.10a)$$

$$\begin{aligned} I_3 &= \int_0^{2\alpha_m} h''(\zeta) h''(\zeta) d\zeta \\ &= 4B^2 \{ 2\alpha_m(1 - \kappa^2)^2 + 4(1 - \kappa^2)(2\kappa^2 - 1)C_2 \\ &\quad + [22\kappa^2(\kappa^2 - 1) + 4]C_4 - 12\kappa^2(2\kappa^2 - 1)C_6 + 9\kappa^4 C_8 \} \end{aligned} \quad (IV.10b)$$

$$I_4 = \int_0^{2\alpha_m} h^3(\zeta) d\zeta = \frac{2\alpha_m^2}{9} \left[\tau I_2 + \frac{6\omega_1}{\alpha_m^3} I_1 \right] \quad (IV.10c)$$

$$I_5 = \int_0^{2\alpha_m} h^2(\zeta) h''(\zeta) d\zeta = -\frac{2\alpha_m^2}{9} \left[\tau I_3 + \frac{6\omega_1}{\alpha_m^3} I_2 \right] \quad (IV.10d)$$

References

1. P.F. Byrd & M.D. Friedman, *Handbook of Elliptic Integrals for Engineers and Scientists*, Springer-Verlag, (1971)
2. W. Chester, "Resonant oscillations in closed tubes", *J. Fluid Mech.*, **18**, (1964), pp. 44-64
3. W. Chester, "Resonant oscillations of water waves. I. Theory", *Proc. Royal Soc.*, **A306**, (1968), pp. 5-22
4. W. Chester & J.A. Bones, "Resonant oscillations of water waves. II. Experiment", *Proc. Royal Soc.*, **A306**, (1968), pp. 23-39
5. W.D. Collins, "Forced oscillations of systems governed by one dimensional nonlinear wave equations", *Quart. J. of Mech. and Applied Math.*, **24**, (1971), pp. 129-153
6. P. Concus, "Standing capillary-gravity waves of finite amplitude: corrigendum", *J. Fluid Mech.*, **19**, (1964), pp. 264-266
7. O. Faltinsen, "A nonlinear theory of sloshing in rectangular tanks", *J. of Ship Research*, **18**, (1974), pp. 224-241
8. J.B. Keller & L. Ting, "Periodic vibrations of systems governed by nonlinear partial differential equations", *Comm. on Pure and Applied Math.*, **19**, (1966), pp. 371-420
9. Y.K. Lou, T.C. Su, & J.E. Flipse, *A Nonlinear Analysis of Liquid Sloshing in Rigid Containers*, Report No. COE-241, Ocean Engineering Program, Texas A&M University, (1980)
10. L. Mack, "Periodic, finite amplitude, axisymmetric gravity waves", *J. Geophysical Research*, **67**, (1962), pp. 829-843
11. B.J. Matkowsky & E.L. Reiss, "Singular perturbation of bifurcations", *SIAM J. Applied Math.*, **33**, (1977), pp. 230-255
12. N.N. Moiseyev, "On the theory of nonlinear vibrations of a liquid of finite volume", *Appl. Math. Mech. (PMM)*, **22**, (1958), pp. 860-870
13. E.L. Reiss, "Imperfect Bifurcation", *Advanced Seminar on Bifurcation Theory*, Math. Research Center, (1977)
14. L.W. Schwartz & A.K. Whitney, "A semi-analytic solution for nonlinear standing waves in deep water", *J. Fluid Mech.*, **107**, (1981), pp. 147-171
15. I. Tajdbakhsh & J.B. Keller, "Standing surface waves of finite amplitude", *J. Fluid Mech.*, **8**, (1960), pp. 442-451

16. G.I. Taylor, "An experimental study of standing waves", *Proc. Royal Soc.*, **A218**, (1953), pp. 44-59
17. J.-M. Vanden-Broeck, "Nonlinear gravity-capillary standing waves in water of arbitrary uniform depth", *J. Fluid Mech.*, **139**, (1984), pp. 97-104
18. J.-M. Vanden-Broeck & L.W. Schwartz, "Numerical calculation of standing waves in water of arbitrary uniform depth", *Physics of Fluids*, **24**, pp. 812-815
19. J.H.G. Verhagen and L. Van Wijngaarden, "Nonlinear oscillations of fluid in a container", *J. Fluid Mech.*, **22**, (1965), pp. 737-751

REPORT DOCUMENTATION PAGE		READ INSTRUCTIONS BEFORE COMPLETING FORM
1. REPORT NUMBER 2878	2. GOVT ACCESSION NO. ADA 163 908	3. RECIPIENT'S CATALOG NUMBER
4. TITLE (and Subtitle) ON THE TWO-DIMENSIONAL PERIODIC SURFACE WAVES OCCURRING IN RECTANGULAR VESSELS: THEORY VERSUS EXPERIMENT		5. TYPE OF REPORT & PERIOD COVERED Summary Report - no specific reporting period
		6. PERFORMING ORG. REPORT NUMBER
7. AUTHOR(s) Thomas J. Bridges		8. CONTRACT OR GRANT NUMBER(s) DAAG29-80-C-0041
9. PERFORMING ORGANIZATION NAME AND ADDRESS Mathematics Research Center, University of 610 Walnut Street Wisconsin Madison, Wisconsin 53705		10. PROGRAM ELEMENT, PROJECT, TASK AREA & WORK UNIT NUMBERS Work Unit Number 2 - Physical Mathematics
11. CONTROLLING OFFICE NAME AND ADDRESS See Item 18 below.		12. REPORT DATE October 1985
		13. NUMBER OF PAGES 74
14. MONITORING AGENCY NAME & ADDRESS (if different from Controlling Office)		15. SECURITY CLASS. (of this report) UNCLASSIFIED
		15a. DECLASSIFICATION/DOWNGRADING SCHEDULE
16. DISTRIBUTION STATEMENT (of this Report) Approved for public release; distribution unlimited.		
17. DISTRIBUTION STATEMENT (of the abstract entered in Block 20, if different from Report)		
18. SUPPLEMENTARY NOTES U. S. Army Research Office P. O. Box 12211 Research Triangle Park North Carolina 27709 National Science Foundation Washington, DC 20550		
19. KEY WORDS (Continue on reverse side if necessary and identify by block number) standing waves cnoidal waves bifurcation experimental observations		
20. ABSTRACT (Continue on reverse side if necessary and identify by block number) This paper is a four part dialectic between theory and experimental observations and measurements of two dimensional periodic surface waves in a vessel of rectangular cross section. The first two parts consist of minor contributions to the existing theory and experimental measurements of elliptic (deep water) standing waves and the (shallow water) travelling hydraulic jump. A new theory is proposed in the third part which explains the transition from the elliptic standing wave to the hyperbolic travelling hydraulic jump. The result is a family of standing cnoidal waves. To lowest order the solution is		

20. ABSTRACT - cont'd.

composed of two non-interacting periodic progressive cnoidal waves travelling in opposite directions. At higher order the two wave trains interact but the interaction produces nothing of qualitative significance except when the cnoidal standing wave of highest amplitude is considered. This family of waves is validated by experimental observation in part four. In addition in part four observation of compound cnoidal standing waves leads to a conjecture about a sequence of continuous wave forms in parameter space leading from the linear sinusoidal wave to the travelling hydraulic jump.

END

FILMED

3-86

DTIC